Journal of Hydrology: Regional Studies 39 (2022) 100976

Contents lists available at ScienceDirect

Journal of Hydrology: Regional Studies

journal homepage: www.elsevier.com/locate/ejrh

Modeling streamflow sensitivity to climate warming and surface water inputs in a montane catchment

K.E. Hale [a,b,*], A.N. Wlostowski [c], A.M. Badger [d,e], K.N. Musselman [a], B. Livneh [f,g], N. P. Molotch [a,b,h]

[a] Institute of Arctic and Alpine Research, University of Colorado, Boulder, CO, United States
[b] Department of Geography, University of Colorado, Boulder, CO, United States
[c] Lynker Technologies, Boulder, CO, United States
[d] Goddard Earth Sciences Technology and Research, Morgan State University, Baltimore, MD, United States
[e] Hydrological Sciences Laboratory, NASA Goddard Space Flight Center, Greenbelt, MD, United States
[f] Department of Civil, Environmental and Architectural Engineering, United States
[g] Cooperative Institute for Research in Environmental Science, University of Colorado, Boulder, CO, United States
[h] Jet Propulsion Laboratory, California Institute of Technology, Pasadena, CA, United States

ARTICLE INFO

Keywords:
Water
Snowmelt
Streamflow
Modeling
Hydroclimatology
Budyko

ABSTRACT

Study region: Gordon Gulch, an upper-montane forest watershed in the Colorado Front Range.
Study focus: As the climate warms, the fraction of precipitation falling as snow is expected to decrease and the timing of snowmelt is expected to shift earlier in spring. In snow-dominated regions, these changes in snow accumulation and melt prompt us to examine downstream changes in streamflow. The objective of this study is to understand how changes in precipitation phase and snowmelt timing alter the timing of surface water inputs (i.e. rainfall and snowmelt) and the partitioning of these inputs between evapotranspiration and streamflow. We used the Distributed Hydrology Soil Vegetation Model and Weather Research and Forecasting Model-based projections of future climatic conditions to simulate streamflow.
New hydrological insights for the region: Modeled annual streamflow decreased by 22% for the period 2071–2100. Surface water inputs increased during winter when atmospheric water demand was relatively low. Subsequently, the winter-period partitioning of water (as rain or snowmelt) to streamflow (as opposed to evapotranspiration) increased, by 15%, while partitioning to evapotranspiration decreased, effectively buffering what would have otherwise been a larger net streamflow decline associated with warming. Seasonal streamflow buffering is unique to snow-influenced systems, as the magnitude and timing of water released from snowpacks is sensitive to warming. This effect may diminish as warming drives snow-influenced systems toward rain-dominance, with implications for hydrological and ecological processes and water-resource management.

1. Introduction

A warming climate is a catalyst for hydrologic change in the mountains, altering seasonal water availability by changing the phase

* Corresponding author at: Institute of Arctic and Alpine Research, University of Colorado, Boulder, CO, United States.
E-mail address: katherine.e.hale@colorado.edu (K.E. Hale).

https://doi.org/10.1016/j.ejrh.2021.100976
Received 30 July 2021; Received in revised form 15 October 2021; Accepted 5 December 2021
Available online 9 December 2021

of precipitation (P) from snow to rain, and the timing of snowmelt (Sturm et al., 2010; Williams et al., 2009). Less snowfall, shallower snowpack, and changes in the timing and magnitude of melt (Mote et al., 2018; Musselman et al., 2017) will alter surface water inputs and the associated partitioning of surface water between evapotranspiration (ET) and streamflow (Q). Overall impacts of climate warming on hydrology have been empirically investigated and modeled, but leave a need to examine individual mechanistic causes to sensitivities in streamflow (Berghuijs et al., 2014; Foster et al., 2016; Gupta and Soroosh, 1998; Hinckley et al., 2012; Kapnick et al., 2018; Livneh and Badger, 2020; Safeeq et al., 2013). An unanswered question in cold region mountain hydrology is how warming may modify the timing of water input to the terrestrial system. We posit that a critical component of hydrologic sensitivity to climate change, due to changes in snowfall and snowmelt, arises from changes in the timing of water delivery to the terrestrial system, broadly defined as the land surface beneath a snowpack. In this context, we define surface water inputs (SWI) as rainfall on the land surface and snowmelt water leaving the base of the snowpack. SWI is thus the sum of liquid water available to the terrestrial system at a given time, which can then be partitioned to streamflow (Q) or evapotranspiration (ET) or enter the subsurface as storage (Brooks et al., 2015; Kiewiet et al., 2021; Kormos et al., 2014). Hence, as the temporal dynamics of either rainfall or snowmelt change with warming, a change in the alignment of SWI and potential evaporation (PET) will occur (Kormos et al., 2014).

In the upper montane forest of the Colorado Front Range, periods of high SWI align with periods of mid to high potential evapotranspiration (PET) (Kormos et al., 2014). Precipitation falls as snow during wintertime months and snow water equivalent (SWE) accumulation stores water until the snowpack melts, creating a lag in the timing between snowfall and SWI generation. The snowmelt period produces a large, sustained pulse of SWI in the spring months, a time of increased PET (Barnett et al., 2005; Brooks et al., 2015; Kampf and Lefsky, 2016; Kormos et al., 2014; Luce et al., 1998; Marks et al., 1998; Milly and Dunne, 2016; Scheff and Frierson, 2014; Sturm et al., 2010). Unlike the higher alpine areas of Colorado mountainous regions, snow accumulation in the montane area studied here is more spatially variable. As a result, snowmelt is not as spatially uniform or as consistent in time as it is in higher elevation areas.

We hypothesize that, within an end-of-current-century warmer climate scenario, the seasonality of catchment SWI and catchment PET may become misaligned, with unknown effects on seasonal streamflow. Under warmer temperatures, SWE accumulation will likely be lower and less persistent throughout the winter, reducing or eliminating the large spring melt pulse (Barnhart et al., 2016; Cayan et al. 2001; Knowles et al., 2005; Kormos et al., 2014; Musselman et al., 2017; Rasmussen et al., 2014; Regonda and Rajagopalan 2004). As snowfall shifts to rainfall and as snowmelt shifts earlier, SWI will shift earlier in the year, during a time of decreased atmospheric water demand (i.e. PET). Previous works have evaluated streamflow sensitivity to climate (e.g., Tennant et al., 2015) but have not identified, mechanistically, the role of changes in the timing of SWI with regard to streamflow production on annual to monthly time scales. To address this knowledge gap, we applied the Distributed Hydrology Soil Vegetation Model (DHSVM) to simulate streamflow under historical conditions and a warmer climate scenario informed by high-resolution weather and climate model runs (Liu et al., 2017). DHSVM was forced with historical metrological data from in-catchment and nearby weather stations (whenever available) and Weather Research Forecast (WRF) model output (to impose warming conditions). We isolated model states and fluxes to estimate how warming-driven changes in the timing of modeled SWI influence catchment streamflow. Analyses specifically included correlations and evaluation of delta values (i.e., the differences in annual and seasonal SWI, ET and Q across model simulations).

When compared against historical conditions, previous modeling studies have reported net decreases in modeled annual streamflow and net increases in annual PET associated with climate warming (Adam et al., 2009; Anghileri et al., 2016; Clow, 2010; Mahanama et al., 2012; Siddique and Palmer, 2021; Tang and Lettenmaier, 2012). Other modeling studies have predicted future increases in wintertime streamflow (Siddique et al., 2021a,b) despite overall annual decreases (Mahanama et al., 2012; Siddique et al., 2020, 2021a,b) and shifts in peak streamflow timing (Tennant et al., 2015). Yet, the mechanism driving the increase in seasonal winter streamflow and its effect on annual hydrologic partitioning remains to be defined and evaluated. We predict that the timing of SWI may change monthly water balance partitioning, providing a much-needed explanation to previous partitioning analyses (Berghuijs et al., 2014; Kormos et al., 2014). To explore potential changes in partitioning, we analyzed DHSVM model output in the context of the Budyko hypothesis (Budyko, 1974), a framework that predicts partitioning of incoming water between streamflow or evapotranspiration based on an index of aridity (PET/P). The following question is addressed: how does climate warming and subsequent changes in the timing of SWI affect monthly and annual streamflow generation and water partitioning within a continental upper montane catchment? We hypothesized that an increase in rainfall and earlier snowmelt events, induced by warming, would temporally decouple catchment water availability (i.e. SWI) and atmospheric water demand (i.e. PET) and thus will increase cold-season hydrologic partitioning to streamflow. Understanding a potential mechanism to changes in annual and seasonal water availability would allow for more accurate water management planning as the climate continues to warm (Mote et al., 2018). The novelty of this study is the model-based quantification of the decoupling of SWI and PET, which isolates SWI as a potential driver of hydrologic change, evaluated through the seasonal changes in modeled winter and early spring streamflow that potentially offset overall reductions in modeled annual streamflow.

2. Study area and methods

We conducted this research in the Gordon Gulch catchment, which is located within the upper montane forest (Marr, 1961) of the Front Range, Colorado, USA (40.0085975°N–105.4411069°W). The period of historical model simulations included the majority of four water years where detailed measurements were available (April 2010–August 2013). A pseudo-warming model simulation was conducted based on a perturbation of the historical period to represent end-of-century climate conditions (Liu et al., 2017). Using DHSVM, we used historical meteorological (air temperature, wind speed, relative humidity, incoming longwave radiation, incoming

shortwave radiation, and precipitation) and streamflow observations to force a control simulation from April 1, 2010 to August 31, 2013. Streamflow data were not available before April 1, 2010, and a regional flood damaged the streamflow gage in mid-September 2013. To emulate warming, we replaced air temperature, relative humidity, incoming longwave radiation for April 1, 2010 to August 31, 2013 with 95-year CMIP5 multi-model ensemble-mean change signal under the RCP8.5 emission scenario from the Weather Research and Forecasting (WRF) model pseudo global warming (PGW) framework (see Liu et al., 2017 for details) to force a warming simulation. After identifying sensitive model parameters in the control simulation and forcing the two simulations within the watershed-scale hydrologic model, we used the Budyko framework (Barnhart et al., 2016; Budyko, 1974; Gerrits et al., 2009; Muleta and Nicklow, 2005; Wang and Tang, 2014) to compare differences in modeled hydrologic partitioning (i.e. ET/P and Q/P) between historical and end-of-current-century model simulations, contrasting the relative seasonal alignment of catchment water supply (i.e. SWI) and atmospheric water demand (i.e. PET) and its effect on streamflow. The details of these methods are described in the

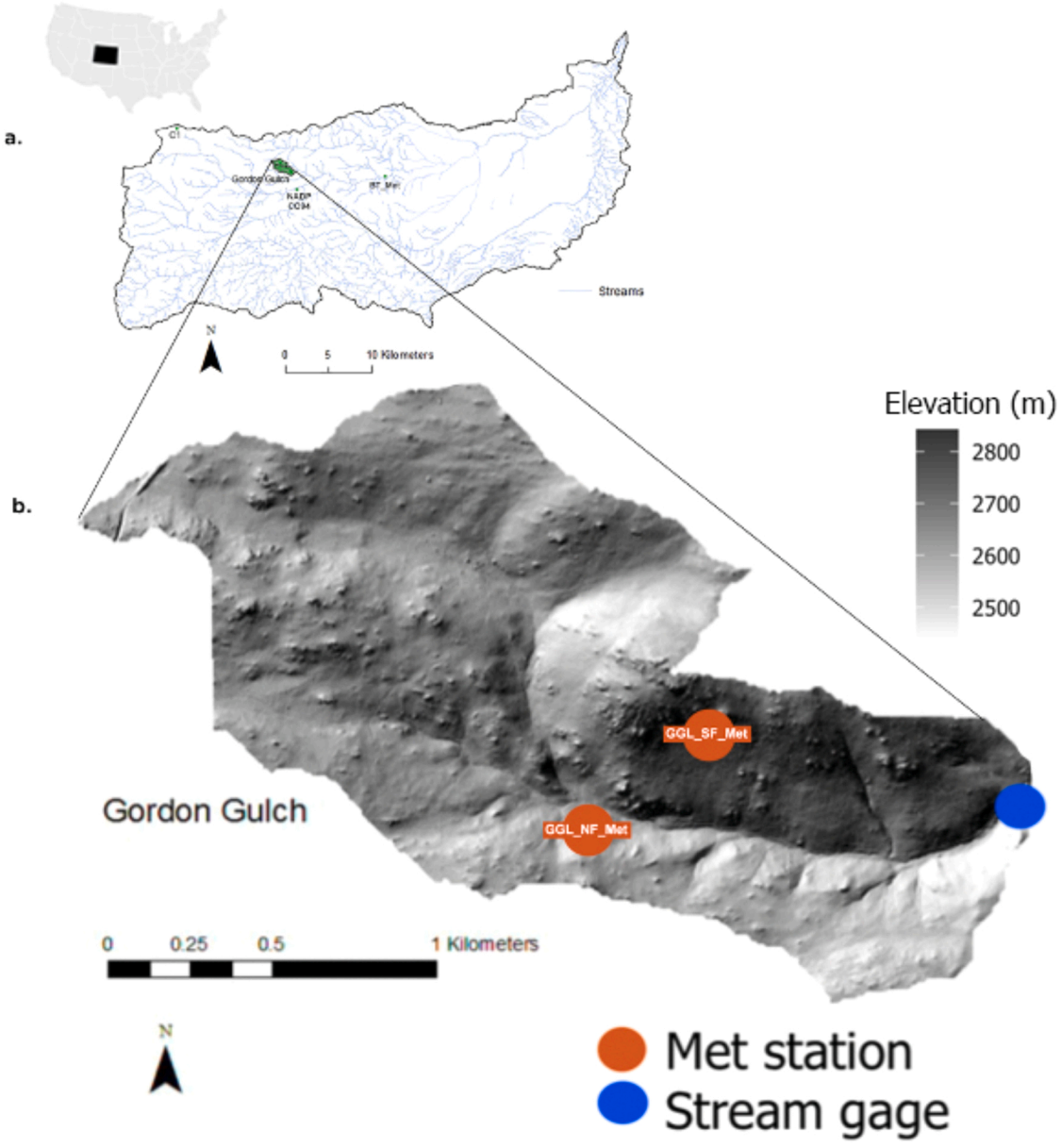

Fig. 1. In North-Central Colorado, (a) Gordon Gulch is an upper montane sub-catchment of Boulder Creek, located 20 km west of Boulder, CO. Meteorological stations near Gordon Gulch include Boulder Creek CZO's BT_Met in Betasso Preserve, National Atmospheric Deposition Program's Sugarloaf CO94 station, and Niwot Ridge C1 (b) Gordon Gulch has two on-site meteorological stations (one on the north facing slope, Boulder Creek CZO's GGL_NF_Met, and one on the south facing slope, GGL_SF_Met) and one streamflow gage. Surrounding the east-west flowing stream are prominent north and south facing aspects.

subsections below.

2.1. Study area: Gordon Gulch, Colorado

This study was conducted in the Gordon Gulch watershed within the Boulder Creek Critical Zone Observatory (BcCZO), 16 km west of Boulder, Colorado. This site was selected for its inclusion in the Boulder Creek Critical Zone Observatory network, where it represents one of few locations where local snow instrumentation, a necessity to this analysis, exists in an upper montane climatic zone, as opposed to strictly in sub-alpine and alpine elevations (many other works in this climatic zone use remotely sensed or data or model output to gain snow information (e.g., Rice et al., 2011; Kelly and Goulden, 2016; Klos et al., 2014; Mainali et al., 2015). Focusing on snow and its temporal release into the terrestrial system in the upper montane forest is important, because the winter season temperatures in this area remain close to 0 °C (Jennings et al., 2018), the snowpack often melts intermittently (Kormos et al., 2014) and is susceptible to small changes in atmospheric conditions, including warming and shifts in precipitation magnitude and phase (Williams et al., 2009). Further, the environmental characteristics and thus hydrologic behavior of Gordon Gulch is, on average, reflective of the behavior in the surrounding upper montane forests in the Colorado Front Range (Anderson et al., 2021), as seen by its "critical zone architecture" which includes soil, mobile regolith, saprolite, and weathered rock.

Gordon Gulch is located within the semi-arid upper montane forest (Fig. 1) and has a catchment area of 2.6 km^2, an average elevation of 2500 m, and an elevation range of 2446 m to 2737 m. The watershed is drained by the eastward-flowing Gordon Gulch stream, with opposing north-south aspect hillslopes (Anderson et al., 2021; Diek et al., 2014). Gordon Gulch experiences seasonal mean temperature differences of 20 °C, with a yearly mean temperature of 5.1 °C. Annual average precipitation is 520 mm, 40%–60% of which falls as snow (Anderson et al., 2021; Anderson and Ragar, 2020a,b,c; Burns et al., 2016; Cowie, 2010). Annual runoff ratios range between 0.08 and 0.23 (Anderson and Ragar, 2020a,b,c; Barry, 1973; Befus et al., 2011; Diek et al., 2014; Hinckley et al., 2012). Gordon Gulch is underlain by gneiss bedrock on which a thin residual soil is developed (Anderson et al., 2021). Soil ranges from 0 m to 0.4 m in thickness (Anderson et al., 2021; Shea, 2013), and seismic refraction profiling shows that reduced seismic velocities corresponding to weathered rock extends to ~ 8-12 m depth across the catchment (Anderson et al., 2021; Befus et al., 2011). The catchment is dotted with tors (i.e. bedrock outcrops), which comprise about 10% of the surface (Anderson et al., 2021). Model forcing and validation data were obtained from a collection of local meteorology stations and spatially gridded data, described below and listed in Table 1, and a streamflow gage within the catchment (Anderson and Ragar, 2020a,b,c).

Table 1
Data sources for the DHSVM control simulation including forcing, vegetation, soil and geology. The datasets were scaled to 20 m, hourly resolutions, using nearest neighbor methodology.

Catchment characteristic	Dataset source	Dataset use and citation and notes	Spatial Resolution	Temporal resolution	Dates gathered
Meteorological forcings (excluding precipitation)	*National Land Data Assimilation System (NLDAS2, phase 2 gridded product)*	Bias corrected air temperature, wind speed, incident shortwave radiation, relative humidity, longwave radiation (Mitchell et al., 2004; Xia et al., 2012)	12 km (1/8 degree)	Hourly	Oct 2000 – Oct 2013
	Gordon Gulch South Facing Meteorology Station (GGL_SF_Met)	Bias correct NLDAS2 for wind speed, incident shortwave radiation (Anderson and Ragar, 2020a,b,c)	Point measurements	10-min	Oct 2012 – Oct 2013
	Gordon Gulch North Facing Meteorology Station (GGL_NF_Met)	Bias correct NLDAS2 for air temperature (Anderson and Ragar, 2020a,b,c)	Point measurements	10-min	Oct 2012 – Oct 2013
	Betasso meteorology station, BT_Met (2000 m, 14.5 km east of Gordon Gulch)	Bias correct NLDAS2 relative humidity (Anderson and Ragar, 2020a,b,c)	Point measurements	10-min	Oct 2010 – Oct 2013
Precipitation	*Gordon Gulch South Facing Meteorology Station, (GGL_SF_Met)*	Used during June-September when available (2012, onwards) (Anderson and Ragar, 2020a,b,c)	Point measurements	10-min	Oct 2000 – Oct 2013
	Betasso meteorology station, BT_Met (2000 m, 14.5 km east of Gordon Gulch)	Used to gap-fill missing GGSF data during June-September (Anderson and Ragar, 2020a,b,c); unheated precipitation gauge until October 2011	Point measurements	10-min	Oct 2000 – Oct 2013
	Sugarloaf CO94 National Atmospheric Deposition Program (NADP, 2500 m, 2 km south of Gordon Gulch)	Used during October-May, gap-filled with C1 data (NADP, 2020); heated precipitation gauge	Point measurements	Daily	Oct 2000 – Oct 2013
	C1 Niwot Ridge (3022 m, 6.5 km west of Gordon Gulch)	Gap fill missing Sugarloaf data using linear relationship (Jennings et al., 2018)	Point measurements	Daily	Oct 2000 – Oct 2013
Streamflow	*Gordon Gulch stream gage, GGL_SW_0_Dis* (Fig. 1)	Full streamflow record, derived from annual stage-discharge relationships (Anderson and Ragar, 2020a,b,c)	Point measurements	10-min	Apr 2010 – Aug 2013
Vegetation	*National Land Cover Database (NLCD)*	Vegetation type (Homer et al., 2015)	30 m	NA	2011
Soil	*Natural Resources Conservation Services (NRCS)*	Soil type (NRCS, 2019)	30 m	NA	2011

2.2. Methods: distributed hydrology soil vegetation model (DHSVM)

DHSVM is a spatially distributed numerical model that uses meteorological forcings and physiographic data to simulate the effects of precipitation, soils, geology and vegetation on the hydrologic response at the catchment-scale (Wigmosta et al., 1994). DHSVM has been used to successfully portray mountainous watershed and sub-watershed processes across North America and to investigate the effects of climate warming and vegetation change on streamflow amount and timing (Livneh et al., 2014, 2015; Raleigh et al., 2016; Westrick et al., 2002; Wigmosta and Lettenmaier, 1999; Yao and Yang, 2009). At each time interval, the model solves energy and water balance equations for every grid cell in the select watershed (Wigmosta et al., 1994) using model forcings (i.e., precipitation, air temperature, wind speed, incident shortwave radiation, relative humidity, and net radiation components), and state variables (e.g., topographic, vegetation and soil characteristics). Model outputs include the primary hydrologic fluxes such as evapotranspiration and streamflow.

A two-layer canopy represents evapotranspiration (ET) and energy transfer at each timestep. A two-layer snow model solves for the snowpack energy and mass balance (e.g., snow accumulation and melt). A multilayer unsaturated soil model and a saturated subsurface flow model simulate subsurface water flow dynamics. PET is calculated using the Penman-Monteith approach. Slope and aspect are accounted for in DHSVM by the characterization of shortwave and longwave radiation within the surface energy budget (Wigmosta et al., 1994). The soil-vegetation water balance in DHSVM accounts for rooting zone water storage, overstory and understory interception, evaporation, and transpiration, surface soil evaporation, snowpack water content, and volume of precipitation (Wigmosta et al., 1994).

DHSVM simulates the exchange of water between grid cells, resulting in a three-dimensional redistribution of surface and subsurface water across the landscape (Wigmosta et al., 1994). DHSVM moves water between grid cells as overland flow, channel flow and/or shallow subsurface flow in the soil. The subsurface water storage in the soil is a function of soil depth and depth to the root zones in each soil layer, where increased soil depth allows for increased storage (McNamara et al., 2005). All through-fall water or snowmelt (that which is not intercepted) enters the soil column and becomes subsurface storage through unsaturated moisture

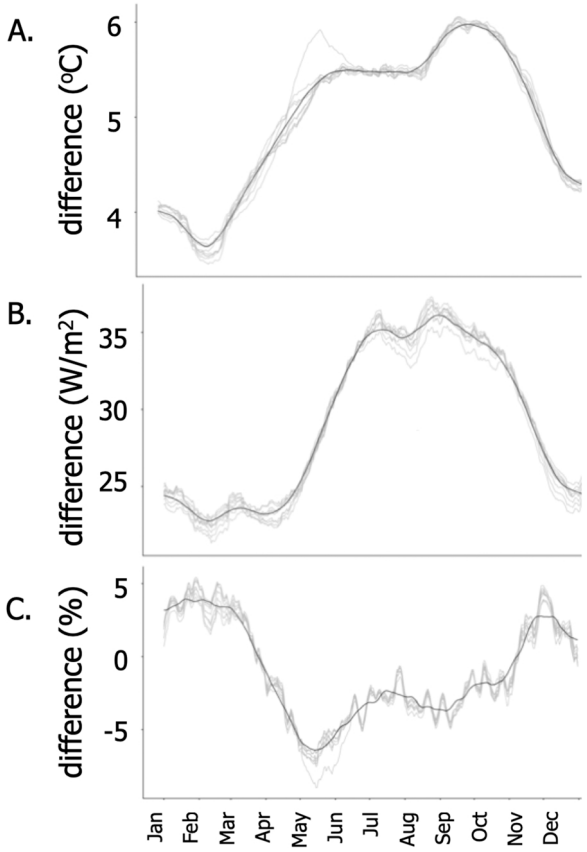

Fig. 2. The average daily difference between the WRF warming simulation (representing end-of-century, 2070-2100, climate) and the WRF historical simulation (representing a present-day climate) in A) temperature (in degrees Celsius); B) longwave radiation (LW, in W/m2) and; C) relative humidity (in %). The difference value represents the daily average value (per variable) of all 9 WRF grid cells (from all 13 WRF pseudoglobal warming simulation years) minus the daily average value (per variable) of the same 9 WRF grid cells (from the present-day historical simulation). The gray lines represent the differences in each variable for each of the 9 WRF grid cells extracted from the Liu et al. (2017) dataset. The black line is a moving 15-day average of each variable and is the value used for the warming simulation.

movement. Once the soil becomes saturated, excess water becomes surface runoff. Thus, soil/vegetation water balance within one grid cell is defined as (see Fig. 2 in Wigmosta et al., 1994):

$$\Delta S_{s1} + \Delta S_{s2} + \Delta S_{s3} + \Delta S_{io} + \Delta S_{iu} + \Delta W = P - E_{io} - E_{iu} - E_s - E_{to} - E_{tu} - P2 \quad (1)$$

where ΔS_{s1} and ΔS_{s2} and ΔS_{s3} are the changes in the three rooting zones soil water storage, respectively. ΔS_{io} is the change in overstory interception and $\Delta S_{iu}$is the change in understory interception. ΔW is the change in snowpack water content, P is the volume of precipitation (rain and/or snow), P2 is the discharge volume leaving the lowest rooting zone, E_s is the volume of surface soil evaporation, and E_{io}, E_{iu}, $E_{to}$and E_{tu} are the volumes of overstory and understory evaporation (from interception storage) and transpiration, respectively.

Via Darcy's law, using the Brooks-Corey Eq. (1), water percolates through the root zones (one defined root zone per soil layer) until discharge from the lower rooting zone recharges the local, grid-cell-specific, water table (Wigmosta et al., 1994; Zhao et al., 2009). Each grid cell then exchanges saturated water with its eight adjacent neighbors (see Fig. 4 in Wigmosta et al., 1994 on subsurface flow routing):

$$q_v(\theta) = KS\left[\frac{\theta - \theta_r}{\phi - \theta_r}\right]^{2m+3} \quad (2)$$

where q_v is the percolation term, *Ks* is the soil vertical saturated hydraulic conductivity, ϕ is the soil porosity, θ_r is the residual soil moisture content, and m is the pore size distribution index. Soil transmissivity is calculated assuming that soil lateral saturated hydraulic conductivity decreases exponentially with depth.

Finally, DHSVM was modified to partition precipitation phase based on the probability of rain or snow at a given time step using a bivariate binary logistic regression (Jennings et al., 2018; Wigmosta and Perkins, 2001; Zhao et al., 2009). Two DHSVM simulations were run at a 20-m resolution on an hourly timestep: a historic/control simulation from April 1, 2010 to August 31, 2013, with a 10-year spin-up period and a warming simulation, representing an end-of-current-century (2070–2100) climate (see Section 2.4).

2.3. Data sources

2.3.1. Meteorological variables

The sources of model input data are listed in Table 1 and include a fusion of in situ measurements from within-catchment stations and nearby stations and meteorological reanalyses from the National Land Data Assimilation System (NLDAS2) (Homer et al., 2015; Mitchell et al., 2004). The purpose of blending these datasets was to build a complete record for the study period, across water years 2000–2013 (which included a 10-year spin-up period from 2000 to 2009). To generate a complete precipitation record, we prioritized the most direct measurements within the Gordon Gulch catchment, whenever available.

In-catchment meteorological stations included the Gordon Gulch north facing meteorological station (GGL_NF_Met*)* and the Gordon Gulch south facing meteorological station *(*GGL_SF_Met*)*. During instances when the in-catchment measurements were not available, nearby meteorological stations were secondarily prioritized, which included the National Atmospheric Deposition Program (NADP) CO94 site (2 km south of Gordon Gulch, elevation of 2390 m), and the Betasso Preserve meteorological station (BT_Met, 10.2 km east, elevation of ~ 2000 m), and Niwot Ridge C1 meteorological station (6.5 km west, elevation of 3022 m). The order in which these different meteorological stations were prioritized to create a complete precipitation record is outlined in Table 1.

The NLDAS2 dataset was prioritized when any remaining gaps in the meteorological record remained (with the exception of precipitation). The NLDAS2 record contains a complete record of all required meteorological model input variables (air temperature, wind speed, incident shortwave radiation, relative humidity, and longwave radiation) and were downscaled from 12 km to 20 m resolution using nearest neighbor interpolation. The NLDAS2 meteorological record for these variables was bias-corrected using the in-catchment and nearby meteorology stations. The bias correction process included: calculating hourly averages of meteorological station observations, which were at a 10-min temporal resolution; finding all instances when meteorological station and NLDAS2 data were both available; fitting a linear model through NLDAS2 data vs. meteorological station data; using linear model parameters to approximate station observations in Gordon Gulch from NLDAS2 record. The order in which different meteorological stations were prioritized to bias correct the NLDAS2 record to create a complete meteorological record (except precipitation) is outlined in Table 1.

2.3.2. Streamflow

There is one streamflow gage in Gordon Gulch, on the eastern end of the catchment (Fig. 1). Streamflow stage is recorded, and streamflow observations (in m^3/s) are derived from existing annual stage-discharge relationships (Anderson and Ragar, 2020a,b,c). Data are available at 10 min intervals and were aggregated to an hourly time series for use in DHSVM.

2.3.3. Vegetation, soil, and geology

Vegetation and soil types were obtained at 30 m resolution from the National Land Cover Database (https://www.mrlc.gov/data?f%5B0%5D=category%3Aland%20cover, accessed: June 2017) and Natural Resources Conservation Services (https://www.nrcs.usda.gov/wps/portal/nrcs/detail/soils/survey/geo/?cid=nrcseprd1464625, accessed: June 2017), respectively. The dominant vegetation types in Gordon Gulch are evergreen forest and shrubs. The dominant soil type is sandy loam Shea (2013). Spatially distributed geology data for the area is available at a 30 m resolution from the USGS. The underlying catchment geology includes: biotite and felsic gneiss, and granite/granitoid/diabase/quartz latite (Anderson et al., 2021). Within DHSVM, these were categorized as metasedimentary and

metavolcanics rocks and intrusive igneous, respectively. The mobile regolith/bedrock interface is located above the water table in Gordon Gulch. The available 30 m vegetation, soil (which includes surface and sub-surface thickness) and geologic data were downscaled to 20 m resolution using nearest neighbor interpolation.

2.4. Model calibration

With the ultimate intent of matching the model streamflow output to the observed streamflow record, to achieve an optimal model configuration, we adjusted a select number of parameterized model soil and vegetation values. The majority of the DHSVM soil and vegetation parameter values were first obtained from a previous application of the model over the Boulder Creek watershed (Badger et al., 2021; Livneh et al., 2014, 2015), since Gordon Gulch lies within this basin and as these past model runs demonstrated realistic simulations of snowmelt and streamflow dynamics.

We then identified an optimal model configuration by adjusting the following five parameters identified as sensitive by previous studies (e.g. Badger et al., 2021; Livneh et al., 2015; Yao and Yang, 2009): hydraulic conductivity, vertical exponential factor, porosity, field capacity and minimum stomatal resistance. The physical relationship between these parameters and streamflow are described below (Section 2.4). 10,000 model runs, with different combinations of values of the select parameters, were sampled following a Latin-Hypercube sampling technique to identify the highest daily Nash-Sutcliffe Efficiency (NSE) value, a coefficient ranging from $-\infty$ to 1 (Breuer et al., 2009; Gan et al., 2014; Livneh et al., 2015; Song et al., 2015). An NSE of 1 indicates a perfect match between observed and modeled datasets, in this case the observed and modeled hydrographs (Manache and Melching, 2004; Nash and Sutcliffe, 1970). Uncertainty within observed streamflow was quantified using 95% confidence intervals within the stage-discharge relationship for each water year. Uncertainty within the simulated streamflow was quantified by including the streamflow output range for the top performing 10% of simulations.

2.4.1. Adjusted parameters for model optimization

Saturated hydraulic conductivity is the rate of water movement through pores of a saturated soil. Thus, hydraulic conductivity is a function of fluid, soil texture and porosity. Saturated hydraulic conductivity *exponentially declines* with depth (see Wigmosta et al., 1994 for details). *Porosity* is the total volume of empty space (voids) to soil material, which influences the amount of water a given volume of soil can hold, in turn influencing the soil moisture at any given timestep. *Field capacity* is the amount of moisture held in the soil after excess water has drained away and the rate of downward movement has decreased. This value is a fraction of the porosity, where a higher field capacity indicates a higher water holding capacity. *Minimum resistance* is a vegetation parameter and it is the opposition to transport water vapor to or from the stomata (pores) on the leaves of plants. The environmental dependencies of the minimum resistance include air temperature, vapor pressure deficit, photosynthetically active radiation flux, and soil moisture (Dickinson et al. 1993; Feddes et al., 1978; Wigmosta et al., 1994), and a higher minimum resistance value means greater opposition toward water movement through stomata. Minimum resistance, per vegetation layer, is a fixed value throughout each model simulation. The parameter values selected for the two model simulations are listed in Table 2, and the limitations introduced by parameter stationarity are discussed in Section 4.1.2.

2.5. Control and warming simulations

We simulated two climate scenarios: a control simulation representing the present-day atmospheric conditions, and a warming simulation representing future atmospheric conditions. The control simulation (2000–2013) was forced with historical data from water years 2000–2013; where 2000–2009 was the 10-year spin-up period and 2010–2013 was the period used for evaluation in this work (data sources are listed in Table 1). This control simulation reflects baseline hydrologic conditions for modeled snow fraction, SWE, SWI, streamflow, and PET. The Penman-Monteith approach, as well as Thornthwaite's temperature-based model (Thornthwaite and Mather, 1955; 1957), were used to estimate PET; the latter method was used for comparative purposes.

The end-of-century (2070–2100) warming scenario was informed by Weather Research and Forecasting (WRF) model output run in

Table 2
Optimized parameters of DHSVM and associated units, value ranges that were tested within Latin-Hypercube sampling optimization, and brief definition. Value ranges were selected based on previous DHSVM calibration (Badger et al., 2021; Livneh et al., 2014, 2015; Yao and Yang, 2009) and field measurements (Anderson and Ragar, 2020a,b,c; Hinckley et al., 2012).

Parameter name	Unit	Manual calibration value ranges	Selected parameter value (spatially uniform)	Definition
Lateral conductivity	m/s	10^{-5} -10^{-2}	0.009	Rate of water movement through soil pores
Exponential factor	m^{-1}	0-5	3	Controls decay of hydraulic conductivity of with depth
Porosity	m^3/m^3	0.4-0.6	0.46	Ratio of void space to total volume
Field Capacity	m^3/m^3	0.18-0.41	0.21	Water holding capacity of soil after drainage
Minimum resistance	s/m	200-700	300	Stomatal opposition of water movement through vegetation pores

a high-resolution, pseudo global warming (PGW) framework by Liu et al. (2017). The work by Liu et al., (2017) includes a 13-year historical reanalysis and a 13-year future climate sensitivity simulation with modified initial and boundary conditions set to the high-end, CMIP5 end-of-century emission scenario as averaged across 19 global climate models (see Liu et al., 2017 for details). The work by Liu et al. (2017) has supported previous assessments of changes in snowpack (Ikeda et al., in review), snowmelt (Musselman et al., 2017), and basin-scale rain-on-snow flood risk (Musselman et al., 2018) for the western U.S. The end-of-century air temperature, relative humidity, and longwave radiation data from Liu et al. (2017) were extracted and averaged for the WRF grid cell encompassing Gordon Gulch and the eight grid cells neighboring Gordon Gulch. Thus, the WRF data were averaged into an hourly dataset for one average water year. Delta values were calculated between the control dataset and the warming dataset, and these delta values were then added/subtracted from the control dataset to generate a warming dataset of equal length as the control dataset.

On average, annual air temperature increased by 4.7 °C (compared to the control simulation), annual longwave radiation increased by 29 W/m^2 and annual relative humidity decreased by 2% (Fig. 2). There is confidence that these variables will change with warming (Gochis et al., 2013) while future precipitation changes are less certain. For this reason, we did not change precipitation amounts in the warming simulation and instead held precipitation constant across simulations; the ramifications of this assumption are discussed in Section 4.1. By assuming that historical precipitation magnitudes will not change in the future climate, we isolated the hydrologic changes associated only with warming, subsequent changes in precipitation phase, and snowmelt timing and magnitude. Thus, relative to our control simulations, our warming experiment permitted an assessment of simulated changes in snowfall fraction, SWE, SWI, PET (Thornthwaite and Mather, 1955, 1957), and runoff (Q) – characterizing the total hydrological impacts of climate warming. Because we are explicitly interested in how warming shifts SWI in the context of water partitioning, we do not consider potential changes in the amount of precipitation as this would not allow us to focus our analyses on our primary questions. Our analysis of warming included monthly and annual comparisons of water and energy variables of interest: rain and snowfall, snowmelt, PET, ET, SWI and Q.

2.6. Budyko analysis of water partitioning

We analyzed DHSVM output and differences in hydrologic partitioning between control and warming simulations within the Budyko framework (Budyko, 1974). The framework requires the following environmental variables for analysis of hydrologic partitioning: precipitation (P), potential evapotranspiration (PET), and evapotranspiration (ET). Based on long-term observations from several catchments globally, Budyko (1974) developed an empirical relationship between catchment evaporative index (ET/P) and its index of aridity (PET/P) (Eq. (3) and Fig. 3):

$$\frac{ET}{P} = \sqrt{\left(\frac{PET}{P}\tanh\left(\frac{P}{PET}\right)\right)\left(1 - \exp\left(-\frac{PET}{P}\right)\right)} \tag{3}$$

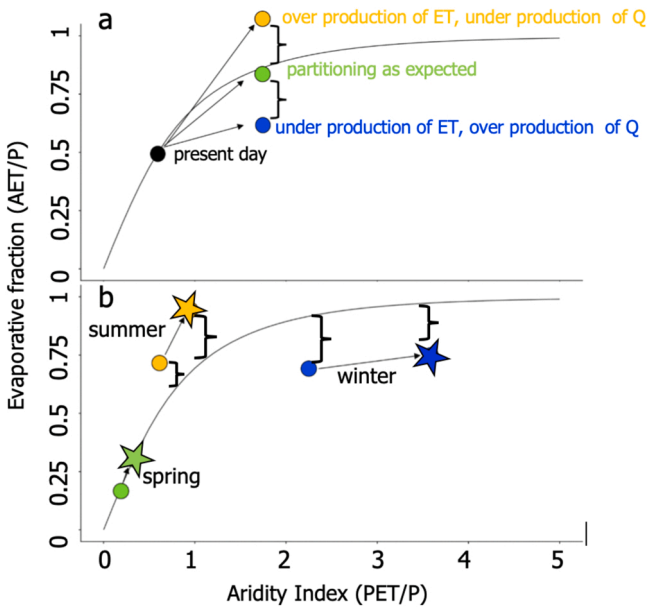

Fig. 3. Conceptual use and interpretation of the Budyko framework on annual and seasonal time frames (a) Hypothetical annual hydrologic behavior of a catchment under control conditions (black point) and warming conditions (yellow, green, blue points) against Budyko's hypothesis (black line). Anomalies from the curve indicate over or under production of ET and Q. (b) Hypothetical seasonal hydrologic behavior of a catchment under control (point) and warming conditions (star). Water and energy limitations are caused by warming and subsequent changes in SWI and water and energy limitations between months. (For interpretation of the references to color in this figure legend, the reader is referred to the web version of this article.)

This framework is broadly used to predict the fraction of precipitation that will be partitioned to streamflow and evapotranspiration (Q/P or 1-ET/P), assuming that changes in ET cause compensatory changes in streamflow (Q) (Berghuijs et al., 2014). The Budyko framework is based on long-term averages and therefore does not consider loss or gain of water via groundwater flow (inter-basin flow), and assumes that there is no change in storage within the catchment, whether in groundwater or soil water. The latter assumption limits the Budyko framework to analysis to annual timesteps, most ideally as longer-term averages. Analyses have been conducted using Budyko over shorter time-scales, in which partitioning behavior must be interpreted in consideration of storage dynamics in the system. Typically, catchments with a low aridity index (PET/P < 1) are energy limited with respect to evapotranspiration, and catchments with a high aridity index (PET/P > 1) are water limited.

Fig. 3a shows the Budyko functional relationship between the aridity index (horizontal axis) and the evaporative index (vertical axis) on a hypothesized seasonal timescale. Anomalies from the Budyko hypothesis result from overproduction of either catchment Q or ET, below and above the line, respectively (Barnhart et al., 2016). Relative to historical conditions (Fig. 3a, black point), water partitioning will change as the aridity index increases in the warming simulation. Water partitioning may change relative to the expectation, which is represented by the Budyko curve. The catchment may partition precipitation to ET and Q under increased aridity index as expected, following the Budyko curve (Fig. 3a, green point). Alternatively, the catchment may partition more precipitation to ET than expected (Fig. 3a, yellow point) or more precipitation to Q than expected (Fig. 3a, blue point).

Comparing hypothetical control and warming conditions (Fig. 3b), it is hypothesized that the warming evaporative index in spring months will increase in magnitude from the control evaporative index, consistent with the Budyko curve without anomalous partitioning (Fig. 3b, point (control) and green star (warming)). In winter months, it is hypothesized that the control simulation (Fig. 3b, blue point) will originally plot below the Budyko curve because atmospheric water demand is low during this time period and therefore any SWI generated by rain or snowmelt is likely to partition more efficiently to streamflow rather than to plant water use, for example. During the winter warming simulation (Fig. 3b, blue star), it is hypothesized that shifts toward earlier snowmelt and from snowfall to rainfall would act to increase winter SWI. This increase in SWI, when atmospheric water demand (i.e. PET) is still relatively low, will act to partition more water to streamflow than expected based on the Budyko curve, yielding an evaporative index value well below the Budyko curve. Lastly, in summer months, it is hypothesized that the control simulation (Fig. 3b, yellow point) may first plot above the Budyko curve, expressing a water-limitation. This is a season of increased atmospheric water demand (PET rises with seasonal temperatures), and the catchment may partition more water to ET. Under warming conditions in the arid western U.S., we hypothesize that summer months will experience the greatest water limitations (Fig. 3b, yellow star). With warming, it is expected that more SWI will occur earlier in the year and less water will persist on the landscape until summer, increasing the existing water-limitation.

We used the Budyko framework on a monthly timeframe to evaluate monthly water and energy limitations and the successive effects on hydrologic partitioning with each consecutive month associated with changes in antecedent moisture availability. Holding precipitation constant, we isolated monthly changes in modeled PET due to warming and evaluated associated increases or decreases in hydrologic partitioning to ET and Q due to changes in monthly SWI. This SWI-focused approach enables a more direct evaluation to how changes in snow accumulation and snowmelt influence hydrologic partitioning. These assumptions allowed us to isolate the relative effects of SWI from total hydrologic partitioning change due to warming by assuming changes in the anomaly from the Budyko curve were the effect of changes in SWI timing and the decoupling of water and energy. Hence, the absolute values represented by the Budyko curve are not important to the analyses, nor are these magnitudes intended to be directly applicable to monthly partitioning in Gordon Gulch, but rather the change in general behavior between simulations (discussed further in Section 4.1).

3. Results

The manual calibration of DHSVM resulted in an NSE value of 0.85 (Fig. 4); an important statistic for verifying adequate model performance (for subsequent results below). This statistic is similar to previous work with DHSVM (Beckers and Alila, 2004; Moriasi et al., 2007; Surfleet et al., 2010; Thyer et al., 2009; van Wie et al., 2013; Wigmosta and Burges, 1997). The simulated runoff ratio was

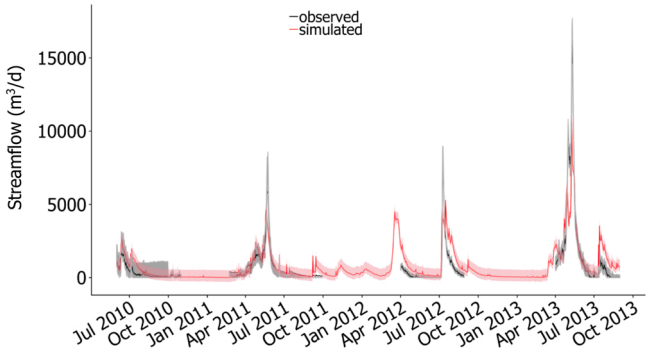

Fig. 4. Streamflow time series in m3/day. Observed Gordon Gulch streamflow (black) bounded by 95% confidence intervals (based on the annual stage-discharge relationship, gray) and DHSVM simulated streamflow (red) bounded by 10% model uncertainty (based on the top performing 10% of all simulations, pink). (For interpretation of the references to color in this figure legend, the reader is referred to the web version of this article.)

0.17, and the observed runoff ratio was 0.16, with an observed uncertainty range from 0.11 to 0.23; i.e. associated with typical uncertainties in the rating curve used to relate measured stage height to discharge. The percent bias, across the entire simulation period, was 37.6%, ranging between 25.3% (in 2013) to 53.7% (in 2011) when evaluated by water year.

3.1. Change in water balance

Annual and average water budget variables from April 1, 2010 to August 31, 2013 are listed in Table 3, including total soil water, total sub-surface flow and average water table depth. Annual precipitation was greater in WY2011 than in WY2012, as was the snow fraction (the fraction of total annual precipitation falling as snow). The greatest change in snow fraction across the control and warming simulations occurred in winter and early spring months where snowfall in the control simulation transitioned to rain in the warming simulation.

Increases in rain and seasonal changes in snowmelt in the warming simulation altered the timing and magnitude of water partitioned as ET and Q (Fig. 5). Because the incoming precipitation amount was fixed across the two simulations, increases or no changes in rain occurred every month of the year, with the greatest increases occurring in April and May (Fig. 5a). As prescribed by our methodology, snowfall decreased in an equal and opposite manner than that of rainfall (Fig. 5b). Snowmelt decreased overall, but increased in December, January and February (Fig. 5c). The increases in rain and melt caused increases in SWI in December and February and in April and May. Conversely, a large decrease in SWI occurred in March (Fig. 5d). As SWI increased in winter months and ET remained low (Fig. 5e), streamflow increased during these months (Fig. 5f). Overall, the catchment experienced an average annual decrease in streamflow of 22%, with a seasonal 15% increase in streamflow during winter and spring months (defined here as November through March).

Evaluating the difference between control and warming monthly average values (i.e. warming value minus control value), there was a statistically significant positive relationship ($p < 0.01$) between ΔSWI and ΔQ where, ΔSWI explained 38% of the variability in ΔQ ($R^2 = 0.38$). Conversely, a statistically significant ($p < 0.01$) inverse relationship between ΔSWI and ΔET, where ΔSWI explained 25% of the variability in ΔET ($R^2 = 0.25$). These results indicate that the change in the timing of SWI has a significant impact on Q and ET, which is consistent with first principles related to water partitioning and associated impacts of seasonal water inputs on energy/water limitations. When including only months when SWI changed by at least 5 mm, a stronger positive relationship ($p < 0.01$) between ΔSWI and ΔQ occurred with an R^2 of 0.48 (Fig. 6a). Similarly, the significantly inverse relationship ($p < 0.01$) between ΔSWI and ΔET also increased when months with SWI changes below 5 mm were excluded; R^2 increased to 0.61 (Fig. 6b). Because we are most interested in the hydrologic response to changes in the timing of SWI, excluding months with minimal SWI change is warranted. Changes in both SWI (Fig. 5d) and Q (Fig. 5f), from the control simulation to the warming simulation, were positive in winter months; these months exhibited increases in rainfall (Fig. 5a) and decreases in snowmelt (Fig. 5c). In spring, both SWI and Q decreased in association with decreased snowmelt (Fig. 5c) and increased ET (Fig. 5e).

There exist monthly nuances to the relationships between changes in SWI, ET, and Q as described above. In April and May specifically, there was a large increase in ET and decrease in Q, but a relatively small change in SWI. In these months, in the control simulation, snowfall and snowmelt occurred in rapid succession. While snow accumulated in late-spring snowstorms, the climate is such that the snow melted shortly afterward, causing little delay in SWI generation (i.e. snowfall and snowmelt occurred in the same month). Similarly, when the catchment was perturbed by the warming simulation and April and May monthly precipitation fell as rain instead of snow, there was no change in the timing of SWI generation at the monthly time scale relative to the control simulation. Given that the snowpack does not store water beyond the monthly time scale in the April and May control simulation, there were little changes in the timing of SWI generation in the warming simulation relative to the control; i.e. because precipitation and SWI occurred in the same month in both simulations. In March, conversely, appreciable snowpack water storage occurred in the control simulation. Hence, in the warming simulation the timing of SWI generation changed in the warming simulation as snowmelt shifted to earlier months (Fig. 5c, February). Lastly, no change in SWI occurred in summer months, as all precipitation fell as rain in both simulations, not affecting the timing of SWI. Notwithstanding, ET and Q both decreased in summer months for the warming simulation, likely because of increased summer water limitations associated with a shift in SWI to winter months and water storage limitations, which are discussed further in Section 4.1.

Table 3
Annual precipitation range, average annual snow fraction and average annual runoff ratio for the control and warming simulations. While precipitation was held constant across simulations, the warming simulation (with differences in temperature, longwave radiation and relative humidity shown in Fig. 2) experienced a decrease in snow fraction and decrease in runoff ratio.

Hydrologic Variable	Control Simulation	Warming Simulation
Annual precipitation range (mm)	459–537	459–537
Average annual snow fraction (%)	36	31
Average annual runoff ratio	0.17	0.12
Sum of water in soil (mm)	18	17
Sum of saturated sub-surface flow (mm)	1169	255
Average water table depth below surface (m)	-1.6e-05	-1.3e-05

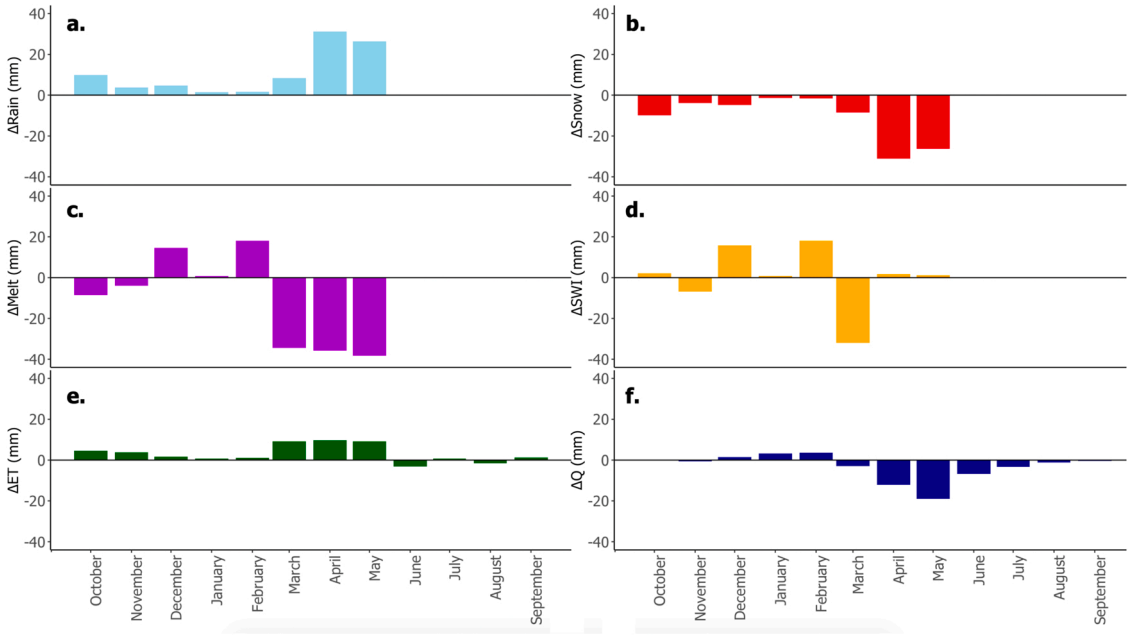

Fig. 5. Differences (in mm/month) in rainfall, snowfall, snowmelt, SWI, ET, and Q between warming and control simulations (a–f, respectively). Positive values indicate greater values in the warming simulation versus the control simulation.

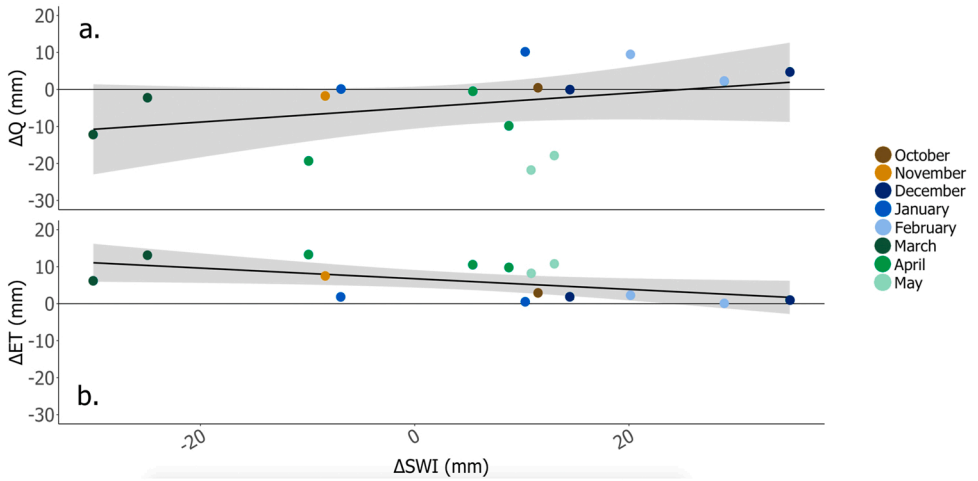

Fig. 6. (a) The relationship between monthly changes in discharge (Q) and surface water inputs (SWI) between warming and control simulations. (b) The relationship between the change in Evapotranspiration (ET) and change in SWI between control and warming simulations. Summer months have been removed for clarity as SWI did not change in summer months.

3.2. Budyko analysis of water partitioning

Under the warming simulation, ET/P increased less than expected from Budyko's function, and therefore decreases in Q/P were less than expected as well (Table 4). ET/P did not increase at the level expected from Budyko because SWI shifted earlier in the year, a

Table 4
Aridity indices, evaporative indices and runoff ratios for control and warming simulations. In the warming simulation, the aridity index increased with a lessened increase in evaporative index and lessened decrease in runoff ratio.

Simulation	Aridity Index (PET/P)	Evaporative Index (ET/P)	Runoff Ratio (Q/P)
Control	1.5	0.83	0.17
Warming	2.85	0.88 (expected ~ 0.92)	0.12 (expected ~ 0.07)

changed that was associated with warming. This change caused winter seasonal increases in Q, which offset the overall annual decrease in Q. According to the Budyko hypothesis, the expected annual average runoff ratio under warming conditions, based on the aridity index calculated from the warming simulation (PET/P = 2.85), was 0.073. The catchment instead experienced an annual average runoff ratio of 0.12, indicating a 4.7% increase in streamflow (i.e. 0.12–0.073) associated with the shift in SWI timing.

Examining the monthly Budyko comparisons illustrated how the modeled water partitioning changed due to warming and changes in SWI timing. In this respect, Fig. 7 shows that under warming, winter months (blue stars) and early spring months (March/April, green stars) plot further below the Budyko curve than the corresponding control simulation (winter months = blue circles, spring months = green circles). Because this time period is primarily energy-limited, the increased SWI exhibited relatively lower partitioning to ET and greater partitioning to streamflow than expected by Budyko. The reductions in ET partitioning (relative to Budyko) are also seen in the water-limited summer months (Fig. 7, red stars versus corresponding red circles). This occurred because shifts toward earlier SWI in previous months increased water-limitations with respect to summer ET. The combined effects of decreased ET partitioning (relative to Budyko) in both winter to early spring months and in summer months resulted in an overall reduction in annual ET partitioning relative to the Budyko expectation. Importantly, one would not expect this type of warming response for a rain-dominated system because shifts in SWI timing would not occur in any month.

In Fig. 8a–d, we show both the raw values and the changes across the control and warming simulations (as a difference value) in average monthly ET/P (Fig. 8a) and SWI (Fig. 8b) to further evaluate the mechanistic impact SWI has on catchment hydrologic partitioning. In the warming simulation, ET/P increases in winter and early spring months and decreases in summer months (Fig. 8c). These changes coincide with water availability (or lack of) in the form of SWI: in the warming simulation, increased SWI is generated in winter months (due to more rainfall and earlier snowmelt events), which caused decreased SWI in later months (i.e., March, Fig. 8d). Similarly, the notable decrease in SWI in March in the warming simulation explains the subsequent decreased ET/P in June, because water-limitations in June are enhanced by the shift toward earlier SWI. Lastly, the notable increases in SWI under warming conditions are seen in the average monthly differences in SWI in December and February. The change in January SWI is less dramatic, as SWI was generally low in the four represented years (averaged in Fig. 8b) and January was likely less sensitive to warming than December and February, as it is climatologically the coldest month in this catchment.

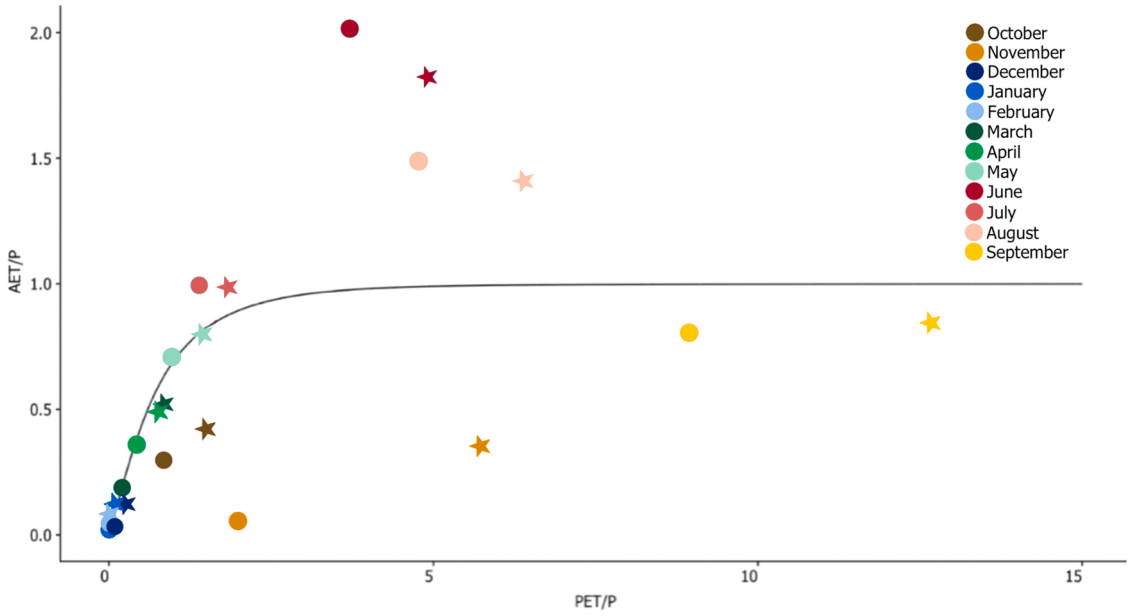

Fig. 7. Monthly aridity indices and evaporative indices within the Budyko space for the control simulation (point) and warming simulation (star). We compared monthly averages between the two simulations. In warming simulation winter months (blue stars) and early-spring months (green stars), the catchment partitions less available SWI to ET and thus more to Q compared to Budyko's hypothesis (black line), plotting vertically lower than the corresponding control simulation (blue circles, green circles) and plotting below Budyko's curve. This is a time of energy-limitation. Conversely, summer months (red circles and corresponding red stars) are water-limited due to a shift toward SWI generation earlier in the year, causing the warming simulation (stars) to plot vertically lower than the control simulation (circles). (For interpretation of the references to color in this figure legend, the reader is referred to the web version of this article.)

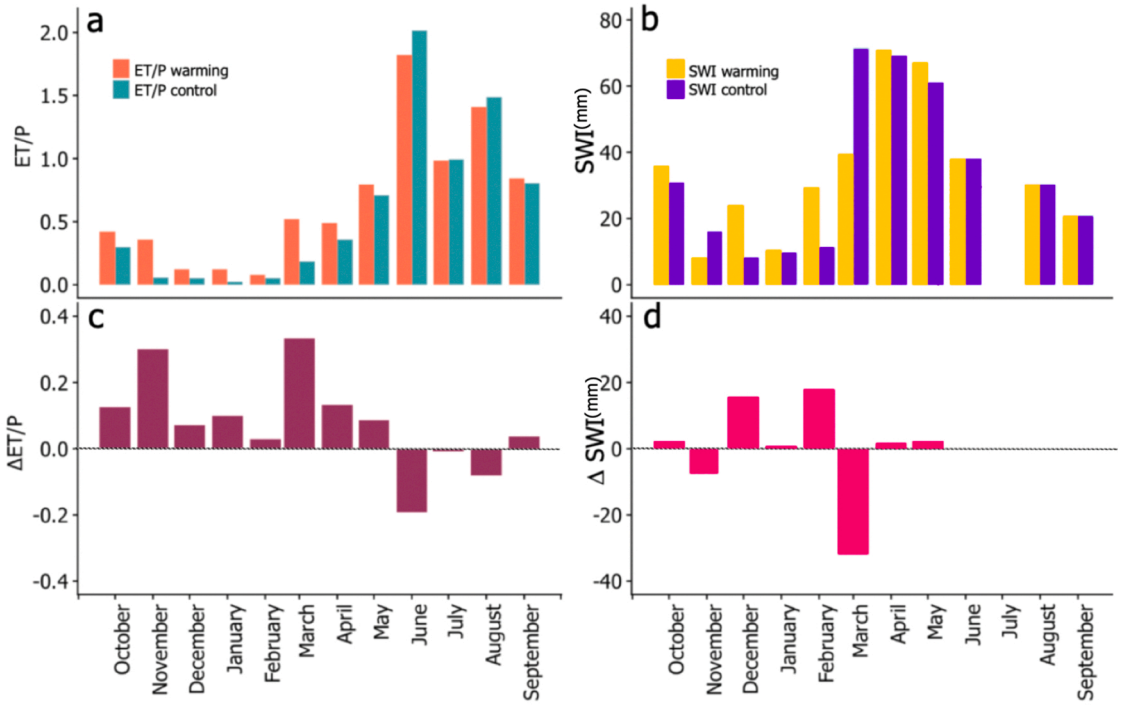

Fig. 8. (a) ET/P and (b) SWI in control and warming conditions. Difference values of (c) average monthly ET/P and (d) average monthly SWI between simulations. Changes in ET/P align with water availability in the form of SWI. Most notably, when ΔSWI is positive, ΔET/P is positive in winter months. ΔET/P is negative in summer months due to water limitations and the input of SWI earlier in the year; e.g. a significant decrease in ΔSWI in March caused a large decrease in ΔET/P in June.

4. Discussion

4.1. Assumptions and limitations

4.1.1. Precipitation

We limited our warming perturbations to air temperature, relative humidity and incoming longwave radiation by amounts shown in Fig. 2. Across the control and warming simulations, we held historical precipitation constant. Allowing precipitation amount to change would have eliminated a means of deciphering how changes in SWI impact ET and Q as changes in precipitation would have also impacted partitioning (Brooks et al., 2015; Kalra and Ahmad, 2011; Wang and Alimohammadi, 2012). Holding P constant in the warming simulation likely created amplified water-limitations in the summertime, where we saw monthly decreases in ET/P.

A number of studies have highlighted uncertainties in future precipitation. By end-of-current-century across the western U.S., Liu et al. (2017) estimated increases in wintertime precipitation between 40% and 70%, with greater increases expected in high elevation mountainous regions. Changes in precipitation during the summer season are less defined and more variable. Kittel et al. (2015) showed that historical precipitation trends on the Front Range of Colorado (1952 to 2010) are unclear as precipitation increased approximately 60 mm per decade at an alpine site (3739 m) but showed no trend at a nearby subalpine site (3022 m). They suggested that precipitation variability is more strongly associated with decadal variability, as both warm-and-wet and warm-and-dry periods will occur in the future. In the greater Upper Colorado River Basin, end-of-current-century precipitation projections are equally unclear, with predictions ranging from a 60% decline at lower elevations to as much as a 74% increase at high elevations (Christensen et al., 2004; Group et al., 2015; Kopytkovskiya et al., 2015; Miller et al., 2014; Minder et al., 2017).

Using this information, we posit that if the wintertime precipitation were to fall as snow, but snowmelt still occurred earlier due to simulated warming, this seasonal increase in precipitation would reinforce our finding regarding a buffering effect associated with a shift in the timing of SWI and associated increases in winter Q. The same result would occur if the future increased wintertime precipitation were to fall as rain, as SWI would be generated immediately in the colder months when PET is relatively low, partitioning more SWI to Q, increasing winter season runoff, and buffering overall annual decreases in Q. Precipitation increases in the future could alleviate catchment water-limitations, and therefore the summer decreases in ET/P noted herein may not be applicable to scenarios of increased precipitation. Irrespective of potential precipitation trends, first principles determine that a shift in SWI will occur with warming and thus the buffering concept revealed here would remain evident. In addition, predictions of future precipitation are highly uncertain and therefore limiting our study to the more certain projections of increased temperature, allows for a more tractable scope in our analyses.

Lastly, the scale and accuracy of precipitation forcing data may have dramatic impacts on streamflow simulations, in particular

extreme peaks. Even at smaller catchment scales, spatial variability of precipitation has been shown to translate into large variations in modeled runoff (Faurès et al., 1995; Goodrich et al., 1995). Thus, in Fig. 4, where the model is unable to accurately capture the runoff peaks observed in Gordon Gulch could be the result of precipitation variability across the catchment that was not represented in the modeled forcing data. This limitation may be improved with high resolution precipitation data and/or including a longer simulation period, which may enhance the model calibration process.

4.1.2. Storage

Additional stationarity was assumed across control and warming model simulations in soil and vegetation parameters. DHSVM was initially optimized in the control simulation to the historic streamflow record, and we assumed that those parameters, which influence sub-surface flow and storage, were transferrable to the future, warming simulation. It is likely that these parameters will change in the next century, introducing a limitation to the methodology used in this work. However, changes in soil properties in particular are likely to occur more rapidly in time, under future warming, to soils high in organic matter, which are less common in Colorado Front Range (which are low in organic matter) (Karmakar et al., 2016). Further, in both simulations, stomatal minimum resistance remains the same throughout one water year (Kaufmann, 1982; Wigmosta et al., 1994), which is not always accurate in a forested area (Irmak and Mutiibwa, 2009).

Next, by evaluating hydrologic partitioning with a monthly scale Budyko analysis, our evaluation of hydrologic storage within Gordon Gulch across months is relative (i.e., we focus on the change in general behavior between simulations). Because the Budyko framework is based on long-term observations, the prediction of an evaporative index from a given aridity index does not consider carry-over in water availability (i.e. storage) from month to month. Thus, when evaluating hydrologic partitioning on a monthly timescale, ET/P can exceed a value of 1, as seen in Fig. 7 and in previous works using the Budyko framework on a shortened, monthly timeframe (Du et al., 2016; 2014; Yokoo et al., 2008; Zhang et al., 2008). Du et al. (2016) address this exceedance by parameterizing water supply as precipitation in addition to root zone water storage change. Thus, because we do not explicitly quantify root zone water storage change in our analysis, we instead assess monthly hydrologic partitioning as relative between our two model simulations, where our results suggest general catchment behavioral differences between a control and warming scenario.

However, water storage in the root zone and water table (i.e., soil and sub-surface storage) can impact the monthly Budyko values by increasing ET (from stored water in the soil and vegetation) in months where P may be low (e.g., control simulation summer months in Fig. 7 when ET exceeds P). Subsequently, once root zone storage is depleted in the semi-arid environment, ET will significantly decrease, despite any P input, as there is no remaining water (e.g., control simulation, fall months in Fig. 7 when ET/P again drops below 1).

4.1.3. Model uncertainties

There are inherent uncertainties in the DHSVM simulations associated with model forcings, parameters, and model structure. Fixed and unfixed parameters attempt to represent an intricate and dramatic landscape and capture environmental micro-dynamics and interactions. However, each parameter introduces an assumption about the landscape, where observations are often lacking (Stewart et al., 2017; Wigmosta et al., 1994; Du et al., 2014; Zhao et al., 2009). This was particularly true with soil parameters, where porosity and field capacity are often poorly known across any given catchment. The representation of the water table bedrock interface within the model (where impermeable bedrock underlies the water table (Wigmosta et al., 1994) also poses a limitation, as it simplifies the underlying structure present in Gordon Gulch, where deep groundwater flow contributes to runoff. The streamflow record of Gordon Gulch also posed limitations to our study, where only three years were available for analysis and model parameter estimation. Owing to the relatively small catchment area (2.6 km^2) and semi-arid climate (520 mm annual precipitation), the streamflow volumes in Gordon Gulch are relatively small and are highly variable; e.g. 2011 was highly snow-dominated (snow fraction 0.53) whereas 2012 was dominated by summer rainfall (snow fraction 0.39). Given these small and variable fluxes, capturing the temporal variability of streamflow within any hydrologic model is challenging.

4.2. Implications

Previous works have suggested that regions with greater proportional snowfall versus rainfall have relatively greater streamflow (Berghuijs et al. 2014; Klos et al., 2014). Such differences across catchments have been attributed to groundwater dynamics and the catchment drainage rate (Safeeq et al., 2013; Tague and Grant, 2009) as well as the rate of snowmelt (Barnhart et al., 2016). As warming shifts surface water inputs from snowfall to rainfall, and causes earlier snowmelt and peak runoff (Tennant et al., 2015), runoff ratios will decrease (Follum et al., 2019; Livneh and Badger, 2020; Zhang et al., 2018). Yet, missing from these preceding assessments of snowmelt-driven changes in streamflow under warming has been an in-depth analysis of how the timing of surface water inputs will change and how this change will impact streamflow generation. The analyses presented herein address this knowledge gap by estimating future changes in hydrologic partitioning associated with an alteration of surface water input seasonality. The shift in SWI caused a 15% increase in winter streamflow which acts as a relative buffer to the 22% annual loss in modeled streamflow.

The resulting overall decrease in annual streamflow with seasonal increases in winter streamflow presented here is complementary to several previous studies. Imposing warming conditions on historical records, both Christensen et al. (2004) and McCabe and Wolock (2016) estimated an end of 20th century annual decrease in streamflow of 17% in the Colorado River Basin. Christensen and Lettenmaier (2006, 2007) estimated an end-of-century annual decrease in streamflow of 8%–11% across the Colorado River Basin. The entirety of western North America is projected, by climate model ensembles and the Variable Infiltration Capacity (VIC) model, to

experience an annual decrease in runoff of 10-30% by 2050 (Christensen and Lettenmaier, 2006, 2007; Milly et al., 2005). Seasonally, Hamlet and Lettenmaier (1999), using the VIC model across the Western United States, saw overall decreases in streamflow but with wintertime increases up to 50% due to increased precipitation. While our results fit within the range of annual streamflow projections, these previous studies leave a need to determine the mechanism for the associated hydrologic changes related to changes in the timing of SWI generation. Past sub-seasonal analyses of hydrologic sensitivity to climate warming have the potential to reveal mechanisms for streamflow change. For example, Foster et al. (2016) evaluated catchment increases in ET and precipitation phase change at two mountainous locations in Colorado, and determined that an increase in ET created larger decreases in Q (compared to precipitation phase changes), suggesting that increases in ET primarily drive decreases in Q.

In this study, winter and spring increases in rainfall fraction and earlier snowmelt events resulted in increased SWI and associated increases in seasonal streamflow. It is also possible that winter and spring SWI increases will recharge groundwater that can support the ET of deep-rooted vegetation, streamflow later in the season, or groundwater export from the catchment. Analyses using the Budyko framework revealed a smaller increase in evaporative index (i.e. ET/P) than expected under a warming scenario (Table 4; Fig. 7 yellow points/stars, green points/stars). In this respect, the anomaly from the Budyko curve increased with warming, resulting in a larger runoff ratio than that expected based on the Budyko hypothesis. As SWI shifted toward winter months, when atmospheric water demand was relatively low, Q/P increased. Such sensitivity of the water balance to the seasonality of climate is consistent with Nasta et al. (2020) and Milly's supply-demand-storage model, demonstrating that when P seasonality and PET seasonality are in-phase, catchments will experience a higher ET/P ratio than when P seasonality and PET seasonality are out-of-phase (Milly, 1994a,b; Nasta et al., 2020; Williams et al., 2012). Temporal differences in the seasonal timing of rainfall caused up to a 20% difference in ET/P, where a longer wetter season (more rainfall in the winter and spring months) caused a lower ET/P and, conversely, greater Q/P and a departure below the Budyko curve (Nasta et al., 2020).

Within a simulated warming climate, streamflow was sensitive to both increased PET and changes in SWI timing, where increased PET acted to decrease Q but earlier SWI acted to increase Q. SWI increased in the winter months when PET was relatively low, decoupling catchment water supply (i.e. SWI) and atmospheric water demand (i.e. PET), and increasing winter streamflow. Under warming conditions, annual mean streamflow still decreased overall but increased in winter, demonstrating how the original presence of snow in the control simulation buffered and offset the overall decrease in Q due to simulated warming. This buffering effect of increased wintertime streamflow is specific to snow-dominated catchments, where buffering of climate sensitivity is associated with shifts in SWI timing. Such sensitivity is buffered until snow longer falls within a catchment, as SWI (produced by solely rainfall) timing will not be affected by warming and no seasonal streamflow climate-sensitivity buffer will exist.

5. Conclusions

In this analysis, the timing of surface water input (SWI) shifted toward earlier in the year due to warming and subsequent decreases in snowfall fraction and earlier snowmelt events. As a result, average annual winter and early spring streamflow (Q) increased by 15%, despite an average annual streamflow decrease of 22%. Hydrologic partitioning within the catchment shifted toward increased ET, but less than would be expected within the Budyko hypothesis. In this regard, winter increases in SWI resulted in a seasonal increase in annual Q relative to the expected value based on Budyko. These wintertime SWI increases caused successive summertime drying, which decreased partitioning to ET/P, when there exist seasonal water-limitations, which were amplified under warming conditions.

To obtain these results, the Distributed Soil Hydrology Vegetation Model (DHSVM) was used to simulate a control and warming scenario, in a small upper montane catchment in the Front Range of Colorado. In order to evaluate solely the effects of SWI on Q, precipitation amount (but not phase) was held constant, and landcover and soil properties were considered stationary across simulations. This approach meant that the model results were most informative when relatively compared against one another, as opposed to presented as absolute, transferrable values. A future study may evaluate annual and seasonal SWI and Q in a non-stationary scenario, where the isolated effect of each variable on Q would need to be identified in order to create a meaningful SWI-Q relationship. We predict that, by first principles, the increased winter season Q as a result of increased SWI from earlier snowmelt would remain.

Overall, the winter-spring streamflow increases and increased Q/P in Budyko space represent a buffering effect with respect to hydrologic sensitivity to climate change that is specific to snow-dominated catchments. As climate warming continues, losses in snow cover may exceed a threshold in which snowmelt becomes an insignificant hydrologic driver and this seasonal streamflow buffering effect will no longer exist. Thus, the findings here represent an expected hydrologic response in near-future conditions within the Colorado Front Range, whereby subsequent responses may reflect more rain-dominated conditions. Critically, the temporal distribution of SWI generation, and future changes, will change where and when water resources will arrive downstream, influencing the reliant, surrounding ecosystems and end-users.

Declaration of Competing Interest

The authors declare that they have no known competing financial interests or personal relationships that could have appeared to influence the work reported in this paper.

Acknowledgements

National Science Foundation, Alexandria, VA, U.S.A, 9810218, 1331872; National Aeronautics Space Administration, Washington D.C., U.S.A, NNH16ZDA001N-WATER, NNH16ZDA001N-THP.

Appendix A. Supplementary material

Supplementary data associated with this article can be found in the online version at doi:10.1016/j.ejrh.2021.100976.

References

Adam, J.C., Hamlet, A.F., Lettenmaier, D.P., 2009. Implications of global climate change for snowmelt hydrology in the twenty-first century. Hydrol. Process. 23 (7), 962–972.

Anderson, S.P., Kelly, P.J., Hoffman, N., Barnhart, K., Befus, K., Ouimet, W., 2021. Is this steady state? Weathering and critical zone architecture in Gordon Gulch, Colorado front range. Hydrogeology, Chemical Weathering, and Soil Formation, pp. 231–252.

Anderson, S., Ragar, D., 2020a. BCCZO – Streamflow / Discharge – Manual (GGU_SW_0_ ManDis) – Gordon Gulch: Upper – (2013–2019), HydroShare. ⟨http://www.hydroshare.org/resource/a69e53f2d272462daccc9901f1914c2c⟩.

Anderson, S., Ragar, D., 2020b. BCCZO – Air Temperature, Meteorology – South-Facing Meteorological Tower (GGL_SF_Met) – Gordon Gulch: Lower – (2012–2019), HydroShare. ⟨http://www.hydroshare.org/resource/d66f1f3239a94c7682c71217b1a94e0b⟩.

Anderson, S., Ragar, D., 2020c. BCCZO – Air Temperature, Meteorology – North-Facing Meteorological Tower (GGL_NF_Met) – Gordon Gulch: Lower – (2012–2019), HydroShare. ⟨http://www.hydroshare.org/resource/d66f1f3239a94c7682c71217b1a94e0b⟩.

Anghileri, D., Voisin, N., Castelletti, A., Pianosi, F., Nijssen, B., Lettenmaier, D.P., 2016. Value of long-term streamflow forecasts to reservoir operations for water supply in snow- dominated river catchments. Water Resour. Res. 52 (6), 4209–4225. https://doi.org/10.1002/2015WR017864.

Badger, A.M., Bjarke, N., Molotch, N.P., Livneh, B., 2021. The sensitivity of runoff generation to spatial snowpack uniformity in an alpine watershed: Green Lakes Valley, Niwot Ridge long-term ecological research station. Hydrol. Process. 35 (9), e14331.

Barnett, T.P., Adam, J.C., Lettenmaier, D.P., 2005. Potential impacts of a warming climate on water availability in snow-dominated regions. Nature 438 (7066), 303–309 https://doi. org/10.1038/nature04141.

Barnhart, T.B., Molotch, N.P., Livneh, B., Harpold, A.A., Knowles, J.F., Schneider, D., 2016. Snowmelt rate dictates streamflow. Geophys. Res. Lett. 43 (15), 8006–8016. https://doi.org/10.1002/2016GL069690.

Barry, R.G., 1973. A climatological transect on the east slope of the front range, Colorado. Arct. Alp. Res. 5 (2), 89–110.

Beckers, J., Alila, Y., 2004. A model of rapid preferential hillslope runoff contributions to peak flow generation in a temperate rain forest watershed. Water Resour. Res. 40 (3) https://doi.org/10.1029/2003 WR002582.

Befus, Kevin, Sheehan, A., Leopold, Matthias, Anderson, Suzanne, Anderson, Robert, 2011. Seismic constraints on critical zone architecture, boulder creek watershed, front range, Colorado. Vadose Zone J. 753, 142010, 10. 915-927. 10.2136/vzj2010.0108.

Berghuijs, W.R., Woods, R.A., Hrachowitz, M., 2014. A precipitation shift from snow towards rain leads to a decrease in streamflow. Nat. Clim. Change 4 (7), 583–586. https://doi.org/10.1038/nclimate2246.

Breuer, L., Huisman, J.A., Willems, P., Bormann, H., Bronstert, A., Croke, B.F.W., Frede, H.G., Gräff, T., Hubrechts, L., Jakeman, A.J., Kite, G., Lanini, J., Leavesley, G., Lettenmaier, D.P., Lindström, G., Seibert, J., Sivapalan, M., Viney, N.R., 2009. Assessing the impact of land use change on hydrology by ensemble modeling (LUCHEM) I: model intercomparison of current land use. Adv. Water Resour. 32, 129–146. https://doi.org/10.1016/j.advwatres.2008.10.003.

Brooks, P.D., Chorover, J., Fan, Y., Godsey, S.E., Maxwell, R.M., McNamara, J.P., Tague, C., 2015. Hydrological partitioning in the critical zone: Recent advances and opportunities for developing transferrable understanding of water cycle dynamics. Water Resour. Res. 51, 6973–6987. https://doi.org/10.1002/2015WR017039.

Budyko, M.I., 1974. Climate and Life. Academic Press, Orlando, FL, p. 508.

Burns, M.A., Barnard, H.R., Gabor, R.S., Mcknight, D.M., Brooks, P.D., 2016. Dissolved organic matter transport reflects hillslope to stream connectivity during snowmelt ina montane catchment. Water Resour. Res. 52, 4905–4923. https://doi.org/10.1002/2015WR017878.

Cayan, D.R., Kammerdiener, S.A., Dettinger, M.D., Captrio, J.M., Peterson, D.H., 2001. Changes in the onset of spring in the Western United States. Bull. Am. Meteorol. Soc. https://doi.org/10.1175/15200477(2001)0822.3.CO;2.

Christensen, N., Lettenmaier, D.P., 2006. A multimodel ensemble approach to assessment of climate change impacts on the hydrology and water resources of the Colorado River basin. Hydrol. Earth Syst. Sci. Discuss. 3, 3727–3770.

Christensen, N.S., Lettenmaier, D.P., 2007. A multimodel ensemble approach to assessment of climate change impacts on the hydrology and water resources of the Colorado River Basin. Hydrol. Earth Syst. Sci. Discuss. 11 (4), 1417–1434.

Christensen, N.S., Wood, A.W., Voisin, N., Lettenmaier, D.P., Palmer, R., 2004. The effects of climate change on the hydrology and water resources of the Colorado River Basin. Clim. Chang. 62, 337–363.

Clow, D.W., 2010. Changes in the timing of snowmelt and streamflow in Colorado: a response to recent warming. J. Clim. 23 (9), 2293–2306. https://doi.org/10.1175/2009jcli2951.1.

Cowie, R.C., 2010. The Hydrology of Headwater Catchments from the Plains to the Continental Divide, Boulder Creek Watershed, Colorado (MA thesis) Geography. University of Colorado.

Dickinson, R.E., Henderson-Sellers, A., Kennedy, P.J., 1993. Biosphere-Atmosphere Transfer Scheme (BATS) Version Leas Coupled to the NCAR Community Climate Model, NCAR Technical Note, NCARITN-387+STR, Boulder, Colorado.

Diek, S., Temme, A.J.A., Teuling, A., 2014. The effect of spatial social variation on the hydrology of a semi-arid rocky mountains catchment. Geoderma 235–236, 113–126.

Du, C., Sun, F., Yu, J., Liu, X., Chen, Y., 2016. New interpretation of the role of water balance in an extended Budyko hypothesis in arid regions. Hydrol. Earth Syst. Sci. 20 (1), 393–409. https://doi.org/10.5194/hess-20-393-2016.

Du, E., Link, T.E., Gravelle, J.A., Hubbart, J.A., 2014. Validation and sensitivity test of the distributed hydrology soil-vegetation model (DHSVM) in a forested mountain watershed. Hydrol. Process. 28 (26), 6196–6210. https://doi.org/10.1002/hyp.10110.

Faurès, J.M., Goodrich, D.C., Woolhiser, D.A., Sorooshian, S., 1995. Impact of small-scale spatial rainfall variability on runoff modeling. J. Hydrol. 173 (1–4), 309–326.

Feddes, R.A., Kowalik, P.J., Zaradny, H., 1978. Simulation of Field Water Use and Crop Yield. John Wiley and Sons, New York, p. 188.

Follum, M.L., Niemann, J.D., Fassnacht, S.R., 2019. A comparison of snowmelt-derived streamflow from temperature-index and modified-temperature-index snow models. Hydrol. Process. 33 (23), 3030–3045.

Foster, L.M., Bearup, L.A., Molotch, N.P., Brooks, P.D., Maxwell, R.M., 2016. Energy budget increases reduce mean streamflow more than snow– rain transitions: using integrated modeling to isolate climate change impacts on rocky mountain hydrology. Environ. Res. Lett. *11*. https://doi.org/10.1088/1748-9326/11/4/044015.

Gan, Y., Duan, Q., Gong, W., Tong, C., Sun, Y., Chu, W., Ye, A., Miao, C., Di, Z., 2014. A comprehensive evaluation of various sensitivity analysis methods: a case study with a hydrological model. Environ. Model. Softw. 51 (1), 269–285.

Gerrits, A.M.J., Savenije, H.H.G., Veling, E.J.M., Pfister, L., 2009. Analytical derivation of the Budyko curve based on rainfall characteristics and a simple evaporation model. Water Resour. Res. 45 (4), W04403.

Gochis, D., et al., 2013. The great Colorado flood of september 2013. Bull. Am. Meteorol. Soc. https://doi.org/10.1175/BAMS-D-13-00241.1.

Goodrich, D.C., Faurès, J.M., Woolhiser, D.A., Lane, L.J., Sorooshian, S., 1995. Measurement and analysis of small-scale convective storm rainfall variability. J. Hydrol. 173 (1–4), 283–308.

Group, M.R.I.E.W., et al., 2015. Elevation-dependent warming in mountain regions of the world. Nat. Clim. Chang 5, 424–430.

Gupta, V.K., Soroosh, S., 1998. Toward improved calibration of hydrological models: multiple and noncommensurable measures of information. Water Resour. Res. 34 (4), 751–763.
Hamlet, A.F., Lettenmaier, D.P., 1999. Effects of climate change on hydrology and water resources in the Columbia River Basin. J. Am. Water Resour. Assoc. 35, 1597–1623. https://doi.org/10.1111/j.1752-1688.1999.tb04240.x.
Hinckley, E., Ebel, B.A., Barnes, R.T., Anderson, R.S., Williams, M.W., Anderson, S.P., 2012. Aspect control of water movement on hillslopes near the rain-snow transition of the Colorado Front Range. Hydrol. Process. https://doi.org/10.1002/hyp.9549.
Homer, C.G., Dewitz, J.A., Yang, L., et al., 2015. Completion of the 2011 national land cover database for the conterminous United States-representing a decade of land cover change information. Photogramm. Eng. Remote Sens. 81, 345–354.
Irmak, S., Mutiibwa, D., 2009. On the dynamics of stomatal resistance: relationships between stomatal behavior and micrometeorological variables and performance of Jarvis-type parameterization. Trans. ASABE 52 (6), 1923–1939.
Jennings, K., Winchell, T., Livneh, B., Molotch, N.P., 2018. Spatial variation of the rain-snow temperature threshold across the Northern Hemisphere. Nat. Commun. 9 (1148), 1148. https://doi.org/10.1038/s41467-018-03629-7.
Kalra, A., Ahmad, S., 2011. Evaluating changes and estimating seasonal precipitation for Colorado River Basin using stochastic nonparametric disaggregation technique. Water Resour. Res. 47, W05555 https://doi.org/10.1029/2010WR009118.
Kampf, S.K., Lefsky, M.A., 2016. Transition of dominant peak flow source from snowmelt to rainfall along the Colorado front range, historical patterns, trends, and lessons from the 2013 Colorado front range floods. Water Resour. Res. 52, 407–422.
Kapnick, S.B., Yang, X., Vecchi, G.A., Delworth, T.L., Gudgel, R., Malyshev, S., Margulis, S.A., 2018. Potential for western US seasonal snowpack prediction. Proc. Natl. Acad. Sci. 115 (6), 201716760 https://doi.org/10.1073/pnas.17167.
Karmakar, R., Das, I., Dutta, D., Rakshit, A., 2016. Potential effects of climate change on soil properties: a review. Sci. Int. 4 (2), 51–73.
Kaufmann, M.R., 1982. Leaf conductance as a function of photosynthetic photon flux density and absolute humidity difference from leaf to air. Plant Physiol. 69, 1018–1022.
Kelly, A.E., Goulden, M.L., 2016. A montane Mediterranean climate supports year-round photosynthesis and high forest biomass. Tree Physiol. 36 (4), 459–468.
Kiewiet, L., Trujillo, E., Hedrick, A., Havens, S., Hale, K., Seyfried, M., Kampf, S., Godsey, S.E., 2021. Stream discharge depends more on the temporal distribution of water inputs than on yearly snowfall fractions for a headwater catchment at the rain-snow transition zone. Hydrol. Earth Syst. Sci. Discuss. https://doi.org/10.5194/hess-2021-362 (In review) [preprint]. https://hess.copernicus.org/preprints/hess-2021-362/#:~:text=We%20found%20that%20stream%20discharge,snow%20due%20to%20climate%20change.
Kittel, T.G.F., Williams, M.W., Chowanski, K., Hartman, M., Ackerman, T., Losleben, M., Blanken, P.D., 2015. Contrasting long-term alpine and subalpine precipitation trends in a mid-latitude North American mountain system, Colorado Front Range, USA. Plant Ecol. Divers. 8, 607–624.
Klos, P.Z., Link, T.E., Abatzoglou, J.T., 2014. Extent of the rain-snow transition zone in the western U.S. under historic and projected climate. Geophys. Res. Lett. 41, 4560–4568. https://doi.org/10.1002/2014GL060500.
Knowles, N., Park, M., Dettinger, M.D., 2005. Trends in snowfall versus rainfall in the Western United States. J. Clim. 9, 1–32. https://doi.org/10.1175/JCLI3850.1.
Kopytkovskiya, M., Geza, M., McCray, J.E., 2015. Climate-change impacts on water resources and hydropower potential in the Upper Colorado River Basin. J. Hydrol. 3, 473–493.
Kormos, P.R., Marks, D., McNamara, J.P., Marshall, H.P., Winstral, A., Flores, A.N., 2014. Snow distribution, melt and surface water inputs to the soil in the mountain rain-snow transition zone. J. Hydrol. 519 (PA), 190–204. https://doi.org/10.1016/j.jhydrol.2014.06.051.
Liu, C., Ikeda, K., Rasmussen, R., Barlage, M., Newman, A.J., Prein, A.F., Chen, F., Chen, L., Clark, M., Dai, A., Dudhia, J., 2017. Continental-scale convection-permitting modeling of the current and future climate of North America. Clim. Dyn. 49 (1–2), 71–95.
Livneh, B., Badger, A.M., 2020. Drought less predictable under declining future snowpack. Nat. Clim. Chang. 10, 452–458. https://doi.org/10.1038/s41558-020-0754-8.
Livneh, B., Deems, J.S., Schneider, D., Barsugli, J.J., Molotch, N.P., 2014. Filling in the gaps: Inferring spatially distributed precipitation from gauge observations over complex terrain. Water Resour. Res. 50 (11), 8589–8610.
Livneh, B., Deems, J.S., Buma, B., Barsugli, J.J., Schneider, D., Molotch, N.P., Wessman, C.A., 2015. Catchment response to bark beetle outbreak and dust-on-snow in the Colorado rock mountains. J. Hydrol. 523, 196–210.
Luce, C.H., Tarboton, D.G., Cooley, K.R., 1998. The influence of the spatial distribution of snow on basin-averaged snowmelt. Hydrol. Process. 12 (10–11), 1671–1683. https://doi.org/10.1002/(SICI)1099-1085(199808/09)12:10/11<1671::AID-HYP688>3.0.CO;2-N.
Mahanama, S., Livneh, B., Koster, R., Lettenmaier, D., Reichle, R., 2012. Soil moisture, snow, and seasonal streamflow forecasts in the United States. J. Hydrometeorol. 13, 189–203.
Mainali, J., All, J., Jha, P.K., Bhuju, D.R., 2015. Responses of montane forest to climate variability in the central Himalayas of Nepal. Mt. Res. Dev. 35 (1), 66–77.
Manache, G., Melching, C.S., 2004. Sensitivity analysis of a water-quality model using latin hypercube sampling. J. Water Resour. Plan. Manag. ASCE 130 (3), 232–242.
Marks, D., Kimball, J., Tingey, D., Link, T., 1998. The sensitivity of snowmelt processes to climate conditions ans forest during rain on snow (SNOBAL).pdf. Hydrol. Process. 1587, 1569–1587.
Marr, John W., 1961. Ecosystems of the East Slope of the Front Range In Colorado. University of Colorado Studies Series in Biology, Boulder, CO, p. 134.
McCabe, G.J., Wolock, D.M., 2016. Variability and trends in runoff efficiency in the conterminous United States. J. Am. Water Resour. Assoc. 52 (5), 1046–1055. https://doi.org/10.1111/1752-1688.12431.
McNamara, J.P., Chandler, D., Seyfried, M., Achet, S., 2005. Soil moisture states, lateral flow, and streamflow generation in a semi-arid, snowmelt-driven catchment. Hydrol. Process. 19, 4023–4038. https://doi.org/10.1002/hyp.5869.
Miller, R.L., et al., 2014. CMIP5 historical simulations (1850–2012) with GISS ModelE2. J. Adv. Model. Earth Syst. 6, 441–477. https://doi.org/10.1002/2013MS000266.
Milly, P.C.D., 1994a. Climate, interseasonal storage of soil water, and the annual water balance. Adv. Water Resour. 17, 19–24.
Milly, P.C.D., 1994b. Climate, soil water storage, and the average annual water balance. Water Resour. Res. 30, 2143–2156.
Milly, P.C.D., Dunne, K.A., 2016. Potential evapotranspiration and continental drying. Nat. Clim. Chang. 6 (10), 946–949. https://doi.org/10.1038/nclimate3046.
Milly, P.C.D., Dunne, K.A., Vecchia, A.V., 2005. Global pattern of trends in streamflow and water availabilty in a changing climate. Nature 438, 347–350 https://doi.org/10.1038/nature04312.
Minder, J.R., Letcher, T.W., Liu, C., 2017. The character and causes of elevation-dependent warming in high-resolution simulations of Rocky Mountain climate change. J. Clim. 31, 2093–2113.
Mitchell, K.E., 2004. The multi-institution North American Land Data Assimilation System (NLDAS): utilizing multiple GCIP products and partners in a continental distributed hydrological modeling system. J. Geophys. Res. 109, D07S90. https://doi.org/10.1029/2003JD003823.
Moriasi, D.N., Arnold, J.G., Van Liew, M.W., Bingner, R.L., Harmel, R.D., Veith, T.L., 2007. Model evaluation guidelines for systematic quantification of accuracy in watershed simulations. Trans. ASABE 50 (3), 885–900.
Mote, P.W., Li, S., Lettenmaier, D.P., Xiao, M., Engel, R., 2018. Dramatic declines in snowpack in the western US. npj Clim. Atmos. Sci. 1 (1), 2. https://doi.org/10.1038/s41612-018-0012-1.
Muleta, M.K., Nicklow, J.W., 2005. Sensitivity and uncertainty analysis coupled with automatic calibration for a distributed watershed model. J. Hydrol. 306 (1–4), 127–145. https://doi.org/10.1016/j.jhydrol.2004.09.005.
Musselman, K.N., Clark, M.P., Liu, C., Ikeda, K., Rasmussen, R., 2017. Slower snowmelt in a warmer world. Nat. Clim. Chang. 7 (3), 214–219 https://doi.org/10.1038/nclimate3225.
Musselman, K.N., Lehner, F., Ikeda, K., Clark, M.P., Prein, A.F., Liu, C., Barlage, M., Rasmussen, R., 2018. Projected increases and shifts in rain-on-snow flood risk over western North America. Nat. Clim. Chang. 8, 808–812. https://doi.org/10.1038/s41558-018-0236-4.

Nash, J.E., Sutcliffe, J.V., 1970. River flow forecasting through conceptual models part I — a discussion of principles. J. Hydrol. 10 (3), 282–290. https://doi.org/10.1016/0022-1694(70)90255-6.
Nasta, P., Allocca, C., Roberto Deidda, R., Nunzio Romano, N., 2020. Assessing the impact of seasonal-rainfall anomalies on catchment-scale water balance components. Hydrol. Earth Syst. Sci. 24, 3211–3227. https://doi.org/10.5194/hess-24-3211-2020.
National Atmospheric Deposition Program, 2020.
Natural Resources Conservation Service, 2019.
Raleigh, M.S., Livneh, B., Lapo, K., Lundquist, J., 2016. How does availability of meteorological forcing data impact physically-based snowpack simulations? J. Hydrometeorol. 17, 99–120. https://doi.org/10.1175/JHM-D-14-0235.1.
Rasmussen, R., Ikeda, K., Liu, C., Gochis, D., Clark, M., Dai, A., Zhang, G., 2014. Climate change impacts on the water balance of the Colorado headwaters: high-resolution regional climate model simulations. J. Hydrometeorol. 15 (3), 1091–1116. https://doi.org/10.1175/JHM-D-13-0118.1.
Regonda, S.K., Rajagopalan, B., 2004. Seasonal cycle shifts in hydroclimatology over the Western United States. J. Clim. https://doi.org/10.1175/JCLI-3272.1.
Rice, R., Bales, R.C., Painter, T.H., Dozier, J., 2011. Snow water equivalent along elevation gradients in the Merced and Tuolumne River basins of the Sierra Nevada. Water Resour. Res. 47, 8.
Safeeq, M., Grant, G.E., Lewis, S.L., Tague, C.L., 2013. Coupling snowpack and groundwater dynamics to interpret historical streamflow trends in the western United States. Hydrol. Process. 27, 655–668.
Scheff, J., Frierson, D.M.W., 2014. Scaling potential evapotranspiration with greenhouse warming. J. Clim. 27 (4), 1539–1558. https://doi.org/10.1175/JCLI-D-13-00233.1.
Shea, N., 2013. Spatial Patterns of Mobile Regolith Thickness and Meteoric 10Be in Gordon Gulch, Front Range, Colorado (MS thesis). University of Connecticut, Storrs, CT.
Siddique, R., Palmer, R., 2021. Climate change impacts on local flood risks in the U.S. northeast: a case study on the Connecticut and Merrimack river basins. J. Am. Water Resour. Assoc. 1–21. https://doi.org/10.1111/1752-1688.12886.
Siddique, R., Karmalkar, A., Sun, F., Palmer, R., 2020. Hydrological extremes across the Commonwealth of Massachusetts in a changing climate. J. Hydrol. Reg. Stud. 32, 100733.
Siddique, R., Mejia, A., Mizukami, N., Palmer, R., 2021a. Impacts of global warming of 1.5, 2.0 and 3.0 °C on hydrologic regimes in the Northeastern U.S. Climate 9 (1), 9. https://doi.org/10.3390/cli9010009.
Siddique, R., Mejia, A., Mizukami, N., Palmer, R., 2021b. Impacts of global warming of 1.5, 2.0 and 3.0 °C on hydrologic regimes in the Northeastern U.S. Climate 9 (1), 9. https://doi.org/10.3390/cli9010009.
Song, X., Zhang, J., Zhan, C., Xuan, Y., Ye, M., Xu, C., 2015. Global sensitivity analysis in hydrological modeling: review of concepts, methods, theoretical framework, and applications. J. Hydrol. 523, 739–757.
Stewart, J.R., Livneh, B., Kasprzyk, J.R., Rajagopalan, B., Minear, J.T., Raseman, W.J., 2017. A multialgorithm approach to land surface modeling of suspended sediment in the Colorado front range. J. Adv. Model. Earth Syst. 9 (7), 2526–2544. https://doi.org/10.1002/2017MS001120.
Sturm, M., Taras, B., Liston, G.E., Derksen, C., Jonas, T., Lea, J., 2010. Estimating snow water equivalent using snow depth data and climate classes. J. Hydrometeorol. 11 (6), 1380–1394. https://doi.org/10.1175/2010JHM1202.1.
Surfleet, C.G., Iii, A.E.S., Mcdonnell, J.J., 2010. Uncertainty assessment of forest road modeling with the distributed hydrology soil vegetation model (DHSVM). Can. J. For. Res. 1409, 1397–1409. https://doi.org/10.1139/X10-079.
Tague, C., Grant, G.E., 2009. Groundwater dynamics mediate low-flow response to global warming in snow-dominated alpine regions. Water Resour. Res. 45 (7), W07421.
Tang, Q., Lettenmaier, D.P., 2012. 21st Century Runoff Sensitivities of Major Global River Basins, pp. 1–5. https://doi.org/10.1029/2011GL050834.
Tennant, C.J., Crosby, B.T., Godsey, S.E., 2015. Elevation-dependent responses of streamflow to climate warming. Hydrol. Process. 29 (6), 991–1001.
Thornthwaite, C.W., Mather, J.R., 1955. The Water Balance. 8. Laboratory of Climatology Publ., Centerton, NJ.
Thornthwaite, C.W., Mather, J.R., 1957. Instructions and Tables for Computing Potential Evapotranspiration and the Water Balance. Drexel Institute of Technology, Laboratory of Climatology, Publications in Climatology, 10(3), p. 311.
Thyer, M., Renard, B., Kavetski, D., Srikanthan, S., 2009. Critical evaluation of parameter consistency and predictive uncertainty in hydrological modeling: a case study using Bayesian total error analysis. Water Resour. Res. 45 (12). DOI: 10.1029/2008 WR006825.
van Wie, J.B., Adam, J.C., Ullman, J.L., 2013. Conservation tillage in dryland agriculture impacts watershed hydrology. J. Hydrol. 483, 26–38. https://doi.org/10.1016/j.jhydrol.2012.12.030.
Wang, D., Alimohammadi, N., 2012. Responses of annual runoff, evaporation and storage change to climate variability at the watershed scale. Water Resour. Res. 48, W05546 https://doi.org/10.1029/2011WR011444.
Wang, D., Tang, Y., 2014. A one-parameter Budyko model for water balance captures emergent behavior in darwinian hydrologic models. Geophys. Res. Lett. 41, 4569–4577.
Westrick, K.J., Storck, P., Mass, C., 2002. Description and evaluation of a hydrometeorological forecast system for mountainous watersheds. Weather Forecast. 17, 250–262.
Wigmosta, M.S., Burges, S.J., 1997. An adaptive modeling and monitoring approach to describle the hydrologic behavior of small catchments. J. Hydrol. 202, 48–77.
Wigmosta, M.S., Lettenmaier, D., 1999. A comparison of simplified methods for routing topographically-driven subsurface flow. Water Resour. Res. 35, 255–264.
Wigmosta, M.S., Perkins, W., 2001. Simulating the effects of forest roads on watershed hydrology, in land use and watersheds: human influence on hydrology and geomorphology in urban and forest areas. AGU Water Sci. Appl. 2, 127–143.
Wigmosta, M.S., Vail, L.W., Lettenmaier, D.P., 1994. A distributed hydrology-vegetation model for complex terrain. Water Resour. 30, 6.
Williams, C.A., Reichstein, M., Buchmann, N., Baldocchi, D., Beer, C., Schwalm, C., Wohlfahrt, G., Hasler, N., Bernhofer, C., Foken, T., Papale, D., Schymansky, S., Schaefer, K., 2012. Climate and vegetation controls on the surface water balance: synthesis of evapotranspiration measured across a global network of flux towers. Water Resour. Res. 48, W06523 https://doi.org/10.1029/2011WR011586.
Williams, M.W., Seibold, C., Chowanski, K., 2009. Storage and release of solutes from a subalpine seasonal snowpack: soil and stream water response, Niwot Ridge, Colorado. Biogeochemistry 95 (1), 77–94. https://doi.org/10.1007/s10533-009-9288-x.
Xia, Y., Mitchell, K., Ek, M., Sheffield, J., Cosgrove, B., Wood, E., Luo, L., Alonge, C., Wei, H., Meng, J., Livneh, B., Lettenmaier, D., Koren, V., Duan, Q., Mo, K., Fan, Y., Mocko, D., 2012. Continental-scale water and energy flux analysis and validation for the North American Land Data Assimilation System project phase 2 (NLDAS-2): 1. Intercomparison and application of model products. J. Geophys. Res. Atmos. 117 (D3), n/a.
Yao, C., Yang, Z., 2009. Parameters optimization on DHSVM model based on a genetic algorithm. Front. Earth Sci. China 3, 364–380.
Yokoo, Y., Sivapalan, M., Oki, T., 2008. Investigating the roles of climate seasonality and landscape characteristics on mean annual and monthly water balances. J. Hydrol. 357 (3–4), 255–269.
Zhang, L., Potter, N., Hickel, K., Zhang, Y.Q., Shao, Q.X., 2008. Water balance modeling over variable time scales based on the Budyko framework–model development and testing. J. Hydrol. 360 (1–4), 117–131.
Zhang, Q., Knowles, J.F., Barnes, R.T., Cowie, R.M., Williams, M.W., 2018. Surface and subsurface water contributions to streamflow from a mesoscale watershed in complex mountain terrain. Hydrol. Process. 954–967. https://doi.org/10.1002/hyp.11469.
Zhao, Q., Liu, Z., Ye, B., Qin, Y., Wei, Z., Fang, S., 2009. A snowmelt runoff forecasting model coupling WRF and DHSVM. Hydrol. Earth Syst. Sci. 13 (10), 1897–1906. https://doi.org/10.5194/hess-13-1897-2009.